An Atlas of the Developing *Drosophila* Visual System Glia and Subcellular mRNA Localization of Transcripts in Single Cells

Amanda A. G. Ferreira[1] and Claude Desplan[1]

1 – Department of Biology, New York University, New York, NY, USA

Abstract

Glial cells are essential for proper nervous system development and function. To understand glial development and function, we comprehensively annotated glial cells in a single-cell mRNA-sequencing (scRNAseq) atlas of the developing *Drosophila* visual system. This allowed us to study their developmental trajectories, from larval to adult stages, and to understand how specific types of glia diversify during development. For example, neuropil glia that are initially transcriptionally similar in larvae, split into ensheathing and astrocyte-like glia during pupal stages. Other glial types, such as chiasm glia change gradually during development without splitting into two cell types.

The analysis of scRNA-seq allowed us to discover that the transcriptome of glial cell bodies can be distinguished from that of their broken processes. The processes contain distinct enriched mRNAs that were validated in vivo. Therefore, we have identified most glial types in the developing optic lobe and devised a computational approach to identify mRNA species that are localized to cell bodies or cellular processes.

Introduction

Glial cells play a fundamental role in brain development and nervous system function. These cells coordinate neural stem cell division, neuronal differentiation, axon pathfinding, and synapse formation (Morante et al. 2013; Fernandes et al. 2017; Poeck et al. 2001; Kim et al. 2020). Glial cells also clean apoptotic cells and cell debris, insulate axons, actively participate in synapses, and constitute the blood-brain barrier (Nakano et al. 2019; Zenker et al. 2014; Gerstner et al. 2012; DeSalvo et al. 2014). Dysfunctional glia are associated with several diseases, such as glioblastoma, Alzheimer's disease, Parkinson's disease, multiple sclerosis, autism, and psychiatric disorders (Ho et al. 2019; Kim et al. 2020).

Anatomically, glia are highly polarized cells having extensive cellular processes in which mRNAs are actively localized in specific subcellular compartments (Carson et al. 2001; D'Arcy and Silver 2020; Herbert et al. 2017). For example, the mRNAs encoding the major myelin protein MBP*,* are found concentrated in the processes of glial cells surrounding the axon they ensheath, and their translation is triggered by activity of the neuron (Wake et al. 2011).

The *Drosophila* optic lobe has four main classes of glia: surface, cortex, neuropil, and nerve-wrapping glia (Chotard and Salecker 2007). Surface glia surround the brain and make up the blood-brain barrier that controls exchanges between the brain and the hemolymph (Desalvo et al. 2011). Cortex glia are in close contact with the neuronal cell bodies and function to nourish neurons and eliminate dead neurons (Nakano et al. 2019). Neuropil glia are associated with neuronal terminals and are essential for synapse formation and neurotransmitter recycling (Omoto et al. 2015; Richier et al. 2017). Finally, nerve-wrapping glia wrap around axon bundles that cross from one neuropil to another, serving as support and protection for these neurons (Chotard and Salecker 2007; Freeman and Doherty 2006). Glial cells are also involved in the development of the nervous system, contributing to axon pathfinding and neuronal circuit assembly. Cortex glia influence neuroblast (neural stem cells in flies) proliferation and differentiation (Morante et al. 2013)(Fernandes et al. 2017; Poeck et al. 2001; Morante et al. 2013). However, the transcriptome of optic lobe glial cells and its changes during development have not yet been investigated. Previous efforts to characterize glial cells in the *Drosophila* brain relied on enhancer traps to identify different glial types based on their morphology (Edwards et al. 2012; Chotard and Salecker 2007).

To comprehensively characterize the transcriptomic diversity of glia in the fly optic lobe, we used scRNA-seq. Optic lobe scRNA-seq datasets at different stages of development were previously obtained in the laboratory and were leveraged to annotate and study glial development from larval to adult stages (Özel et al. 2021; Konstantinides et al. 2022). About 32,000 sequenced optic lobe glial cells from larvae, four pupal stages, and adults were analyzed. We annotated most glial cells and validated these annotations

at the third instar larval (L3) and adult stages. Their cell identities were then transferred to all pupal stages by integrating the datasets. mRNA expression of the classical glial marker *repo* is low and is thus insufficient to identify all glial clusters in scRNAseq datasets. However, we identified three new genes (*CG32032*, *AnxB9*, and *GstE12)* that served as universal glial markers. Glia differentiated through three different trajectories according to the integration: (1) cells whose transcriptome minimally changed from larvae to adults, such as cortex and perineurial glia; (2) cells whose transcriptome gradually changed and formed a linear trajectory, like inner and outer chiasm glia; and (3) cells that formed an initial linear trajectory and then split into at least two different fates, such as medulla neuropil and lamina neuropil glia (epithelial/marginal). Moreover, while analyzing these scRNA-seq datasets, we discovered that glial cells were broken down into different cell fragments during cell dissociation that were then sequenced independently and clustered separately from their cell bodies: Unique glial cell types are thus represented by multiple clusters corresponding to the cell bodies and cell processes with distinct mRNA contents.

Results

Identification of new glia-specific genes

Marker genes are essential in order to identify glial clusters in scRNA-seq datasets. In *Drosophila*, glial cells are most often defined *in vivo* by the expression of the Repo protein (Halter et al. 1995). To identify glial clusters in scRNAseq, the larval clusters (Konstantinides et al. 2022) whose transcriptome exhibited a high correlation with the transcriptome of fluorescence-activated (FAC)-sorted cells based on the expression of a *repo* GFP transcriptional reporter, and a low correlation with that of neurons FACSorted based on Elav protein (a pan-neuronal marker) expression were selected, as previously done in the adult optic lobe dataset (Özel et al. 2021) (Fig 1A and S1A).

Although the glial clusters expressed the *repo* GFP reporter, the endogenous *repo* mRNA was lowly expressed and often absent in many of these glial clusters: *repo* mRNA was only strongly expressed (average expression per cluster greater than 0.5) in 11 out of 23 larval clusters and in 5 out of 21 adult clusters (Fig. 1B-C). This low transcript detection in scRNA-seq experiments is probably due to ‘dropouts’ that are common for lowly expressed genes (Qiu 2020; Phipson et al. 2017). Consequently, the absence of *repo* expression in glial clusters in scRNA-seq data may result in many clusters mistakenly not being considered glial cells. For example, in the larva, both types of surface glia (subperineurial - spg and perineurial – pg) had low *repo* expression levels in the dataset (cluster 21 for subperineurial, and 8 and 14 for perineurial), which correlates to the low detection of *repo* mRNA by Hybridization Chain Reaction RNA Fluorescence *in situ* Hybridization (HCR RNA FISH) (Choi et al. 2018; Schwarzkopf et al. 2021) even if

these cells could easily be identified as glial cells by antibody detection of the Repo protein (Fig. S1B).

To overcome this challenge, we looked for other more highly expressed specific glial genes that could allow us to identify glia in scRNA-seq datasets, independently or together with *repo* expression. By comparing all the larval glial clusters with the remaining clusters (non-glia), several genes were identified that were differentially expressed in glial cells as compared to neurons: *Ama*, *MtnA*, *AnxB9*, *CG32032*, *CG7433*, *GstE12*, *CG9686*, *CG15209*, and *Npc2a* (Fig. S1C-E). Among these genes, *AnxB9*, *CG32032* and *GstE12* were individually expressed in most glial clusters, including those that did not express *repo* (Fig. 1A, B, Fig. S1E) but were largely absent in neuronal clusters, with few exceptions; for instance, *AnxB9* was expressed in clusters that did not express any of the other glial markers, which were then not considered glia (Fig. S1F-G). *AnxB9* belongs to the family of annexins that bind to phospholipids and participate in membrane remodeling, membrane trafficking, and exocytosis (Mirsaeidi et al. 2016). Annexins are widely found in the nervous system and show different expression patterns in neurons and glia (Eberhard et al. 1994; Solito et al. 2008). *CG32032* belongs to the calycin protein superfamily (FlyBase), which includes lipocalins and fatty acid-binding proteins often found in glial cells, such as the human *FABP7* and *PMP2* (Kaloshi et al. 2007; Zenker et al. 2014). Finally, *GstE12* encodes a cytoplasmic enzyme involved in glutathione metabolism (Saisawang et al. 2012). In mice, astrocytes enhance proinflammatory response in the brain through Glutathione S-transferases because the knockdown of these enzymes in astrocytes compromises microglial activation (Kano et al. 2019).

Thus, *CG32032*, *AnxB9,* and *GstE12* are all expressed strongly and mostly specifically in glia and thus, in combination with *repo*, are good candidates for the identification of glial cell identification in scRNA-seq datasets. Based on the expression of at least two of these genes, all previously identified glial clusters in both larval (23 out of 23 clusters) and adult (21 out of 21 clusters) datasets were identified, and none of the non-glial clusters expressed these combinations. Immunohistochemistry studies confirmed that the protein product of *CG32032* and *AnxB9* genes were present in glial cells in both L3 larvae and adults (Fig. 1D-E).

To test whether these genes could help identify new glia in other datasets, we analyzed their expression in a published optic lobe scRNA-seq dataset from pharate adults (96 hours pupation – P96) (Kurmangaliyev et al. 2020). *Repo* was lowly expressed in three clusters annotated as glia by the authors (Fig. S1F). However, these three clusters expressed at least two of the new glial markers. Moreover, the dataset contained clusters called “C clusters” that were annotated neither as glia nor as neurons (Fig. S1F). Many of the cells in these “C clusters” expressed the new glial markers. Indeed, out of all 321 cells in the “C clusters”, 103 had transcriptome that correlated with adult subperineurial glial cells. Similarly, cluster N183, previously annotated as an unknown

neuronal cluster, also showed expression of the new glial markers and was composed of 19 cells, of which 9 also correlated with subperineurial glial cells. Another published *Drosophila* scRNA-seq dataset of the ventral nerve cord (VNC) was also analyzed (Allen et al. 2020). Two of the clusters that the authors had identified as glia/neuron mix due to low expression of *repo* could be confidently identified as glia when using the combined expression of *repo*, *CG32032*, *AnxB9,* and *GstE12* (Fig. S1F). Later, the authors managed to identify these clusters as glia, based on specific glial subtypes markers (Allen et al. 2020). In summary, using four different datasets, we showed that *repo*, *CG32032*, *AnxB9,* and *GstE12* are marker genes that can be used to identify glial clusters in *Drosophila* scRNA-seq datasets.

Annotation of glial clusters in a developmental scRNA-seq atlas of the fly optic lobe

After establishing universal glial markers, we sought to evaluate glial diversity in the larval and adult stages. High-resolution transcriptomic atlases of the optic lobe throughout development (Özel et al. 2021; Konstantinides et al. 2022) had identified more than 200 cell types, including progenitors, neurons, and glia. In these datasets, glial clusters were not annotated as specific glial types. We excluded neurons and reclustered the remaining cells: This allowed us to annotate the different glial cell types based on genes that were differentially expressed among different glial subtypes (Simon and Konstantinides 2021). As glial cell bodies occupy stereotypical positions in the brain, this allowed us to validate their identification based on their soma position in the optic lobe and the expression of the Repo protein. We annotated and validated larval clusters based on known (McMullen et al. 2021; Hofmeyer et al. 2008; Cameron et al. 2016; Matthews et al. 1990; Nakano et al. 2019; Edwards et al. 2012; DeSalvo et al. 2014; Konstantinides et al. 2018; Chen et al. 2016; Chotard and Salecker 2007; Chotard et al. 2005; Spéder and Brand 2018; Richier et al. 2017) or new markers (summarized in Table 1 and Methods) and their cell body positions using transcriptional reporters, protein traps, enhancer traps, antibodies, as well as specific HCR RNA FISH probes (Fig. 2A-B, Fig. S2, and Table 1).

At the adult stage, we based our annotations on cell-type specific markers established by earlier studies that had identified genes expressed in specific subtypes of glia using enhancer traps, antibody staining, cell-type specific RNA-seq, and scRNA-seq (Brunet Avalos et al. 2019; Konstantinides et al. 2018; Huang et al. 2015; Croset et al. 2018; Davie et al. 2018; Richier et al. 2017; DeSalvo et al. 2014; Romero-Calderón et al. 2008; Davis et al. 2020). We determined the identity of adult clusters by taking advantage of the spatial distribution of glial cells combined with immunohistochemistry for genes that were expressed in one or a few clusters (Fig. 2C-D and Fig. S3) (See Table 2 for the list of markers, annotations, and corresponding references). Ultimately, we could assess the transcriptome of all glial cell types and determine specific markers for each of them (Table

S1). This represents a powerful tool for studying glial cells and their contribution to the development and function of the optic lobe.

Developmental trajectories of glial cells from larva to adult stages

Since the glia transcriptome changes over time, we investigated how glial cell diversity increases during development, from larva (10 subtypes) to adult (19 subtypes). To do that, we integrated all glial cells from larvae, P15 (15 hours after pupation), P30, P50, P70, and adults into one dataset (Fig. 3A). The larval glial cells annotations were performed independently of adult annotations. Yet, the same cell types across stages clustered together, such as cortex, perineurial, subperineurial, lamina neuropil, medulla neuropil, inner and outer chiasm glia (Fig. 3B, C). The transcriptomic similarity of the same cell types throughout development corroborates the robustness of our marker-based cell type annotation (Tables 1 and 2).

Strikingly, we observed three distinct types of developmental trajectories based on our integrated dataset:

(1) cells that did not exhibit a trajectory (*i.e.* minimally changed) from larvae to adults, such as cortex and perineurial glia. These are cells that maintain a similar role throughout development (Fig. 3A, black circles).

(2) cells that gradually changed their transcriptomes in a linear trajectory throughout developmental stages, like inner and outer chiasm glia, thus likely maturing during this process (Fig. 3A, blue arrows). Besides chiasm glia, we also observed cell types with different nomenclatures in the larvae and adults but that were previously shown to be the same cell by lineage-trancing experiments (Edwards et al. 2012). For example, in adults, there are two satellite glia in the lamina, named proximal and distal (Kremer et al. 2017), but only one satellite glia is found in larvae. The larval satellite glia gradually mature to become proximal satellite glia in adults. In contrast, the adult distal satellite glia have a different origin, corresponding to larval retina wrapping glia (Edwards et al. 2012), which is a nerve-wrapping glial type in larvae that is repurposed to work as a cortex type in adults. (Fig. 3B, C).

(3) cells that form an initial linear trajectory and then split into at least two different cell fates (Fig. 3A, red arrows).

- For instance, medulla neuropil glia are composed of at least two different subtypes in adults, ensheathing glia (EG) and astrocyte-like (ALG), which share the same origin as larval medulla neuropil glia. These glia originate from the last division of neuroblasts in the outer proliferation center (OPC) (Li et al. 2013). They showed a single trajectory, being transcriptionally similar from larva to P30 but then splitting into two different trajectories leading to EG and ALG after P30 (Fig. 3D and S4A).
- Similarly, the lamina neuropil glia, epithelial (ensheathing) and marginal (astrocyte-like) glia in adults originate from the same precursors in the larva, in a region of the OPC called

glia precursor cell area (Chen et al. 2016). They could not be separated transcriptionally into distinct cell types in larvae, whereas they split into separated trajectories starting at P30 (Fig. 3A-C). This suggests that at the time of their birth, these lamina neuropil glial cells were formed a single cluster with transcriptionally indistinguishable cells, and could only be defined as distinct cell types during their maturation at metamorphosis, leading to expanded cell diversity in the adult as compared to the larva. The same things appears to affect medulla neuropil glia.

- Interestingly, glia in the lobula complex neuropil in larvae (which later separates into lobula and lobula plate), seems to develop in a different manner than what we found for medulla and lamina neuropil glia. We found at least two different origins for the lobula complex neuropil glia:

First, we annotated and validated one cluster as lobula complex neuropil glia in the larva (Fig. S2A, D, and H – lobula c. neuropil). However, different from the other larval neuropil glia, this cluster already expressed mature astrocyte-like glia markers in the larva and their cluster in the integrated data was positioned between adult medulla astrocyte-like glia and another unknown adult astrocyte-like clusters (Astrocytes_1, 2, 3 and 4, Fig. 3A, E and S4B). This suggests that the lobula complex neuropil glia found in the larva are already mature cells. Mature astrocyte-like glia can also be found in the larval central brain that is physically closely associated with the lobula complex in larvae. Therefore, the lobula complex glia cluster found in the larval dataset differs from the other optic lobe neuropil glia in their stage of maturation.

Second, we found a new trajectory starting at P15 that is at the origin of an unknown ensheathing glia cluster, which likely contains lobula and lobula plate ensheathing glia. We looked for genes that were commonly expressed in larvae in both medulla and lamina neuropil glia. Out of the 61 genes found to be commonly expressed in the early trajectory of both medulla neuropil and lamina neuropil glia (Table 3), six of them were unique and mostly absent in other glial types: *CR30009, gcm, E(spl)mgamma-HLH, CG11670, E(spl)malpha-BFM, Traf4* (Fig. S4C-H). Interestingly, these genes were not expressed in the mature larva lobula complex neuropil glia cluster (lobula complex neuropil) but were expressed at the beginning of the unknown ensheathing glia trajectory (Fig. 3E and S4B-K, labeled “another lobula/lobula plate neuropil glia?”). Although there were no corresponding glial clusters at the larval stage, cells from P15 could be identified in this unknown neuropil glia (Fig. 3A and E – orange cells). Unique markers to validate the identity of these cells in adults were not found, but we hypothesize that they are part of the lobula and lobula plate neuropil glia. This is due to the fact that we have confidently annotated all glial types but could not find lobula and lobula plate neuropil glia in adults; by elimination, the unannotated glial clusters that form a separated trajectory from the medulla neuropil glia are lobula and lobula plate neuropil glia.

Finally, there were three clusters of surface lamina glia for which we could not identify contributions from larva glia: pseudocartridge (a subtype of subperineurial glia) as well as fenestrated and chalice glia, which are both subtypes of perineurial glia (Fig. 3A-C, dashed circles). Pseudocartridge and fenestrated glia and likely chalice glia (Kremer et al. 2017) originate from the eye disc (Edwards and Meinertzhagen 2010) that was not sequenced in the larva dataset (Konstantinides et al. 2022), thus explaining their absence (summarized on Table S3).

Together, our data show that the increased number of adult glial clusters compared to the larval dataset is, in part, the result of increased glial cell diversity from transcriptionally similar neuropil glia in larvae to different subtypes in adult.

scRNA-seq reveals subcellular distribution of RNAs

Next, we sought to investigate three surprising observations in the larval dataset:

- First, we found a cluster of retina wrapping glia (Fig. 2A, Fig. S2J) that was unexpected since their cell bodies are located in the eye disc that was dissected out from the larval optic lobe before sequencing (Konstantinides et al. 2022) (Fig. 4A), in contrast with the absence of the other eye-disc glia (chalice, pseudocartridge, and fenestrated, see above). Interestingly, the retina wrapping glia are the only eye-disc glia that extends their processes into the optic lobe. Therefore, we hypothesized that cell processes that were broken off the cell body could form fragments that were sequenced and contain enough mRNA to form clusters of defined cell identities.

- Second, we found an extra chiasm cluster that could also be explained by the sequencing of cellular processes since this glial type also have long and extensive cellular processes (Fig. 4B) that could be fragmented and sequenced as unique “cells”. For chiasm glia, at larval stages, unsupervised clustering revealed two chiasm clusters: Cluster 12 that could be separated with supervision and annotated as inner and outer chiasm (Fig. S2A and Fig. 5A), the only two known types of chiasm glia in the optic lobe (Tix et al. 1997). On the other hand, cluster 4 shared all the top chiasm glia markers with cluster 12 (Fig. S5B), suggesting that cluster 4 was not a different third type of chiasm glia. We thus hypothesized that cluster 12 was comprised of cell bodies with nuclei (Chiasm_CB), while cluster 4 was comprised of processes without nuclei (Chiasm_PC) (Fig. S5A-B).

There were two striking differences between the putative chiasm cell body and the putative chiasm processes clusters. First, the Chiasm_CB cluster contained cells with significantly more molecules of RNA (UMIs) than Chiasm_PC (Fig. 4D); second, only Chiasm_CB contained mRNA for the transcription factor (TF) Repo (Fig. 4E) and the combined content of all TFs was significantly higher in Chiasm_CB compared to Chiasm_PC (Fig. 4F). In contrast, Chiasm_PC presented higher levels of *Act5C* (Fig. 4G) and *FK506-bp2* (Fig. 4H) as well as other genes previous described as having a specific

sub-cellular localization to cell extensions (Table S2). For example, the closest human ortholog of *Act5C* is *β-actin*, the first gene to be shown to have its mRNA subcellularly distributed and be transported to the neurites of neurons and lamellipodia of migrating fibroblasts (Condeelis and Singer 2005; Jeffery et al. 1983; Zhang et al. 2001; Martin and Ephrussi 2009). *FK506-bp2* is a member of a highly conserved family of immunophilins that are enriched in neurites in mammalian neurons (Kügelgen and Chekulaeva 2020).

To strengthen our hypothesis, reads mapping to introns or exons were compared in both chiasm clusters. Since unspliced mRNAs and introns are essentially present only in the nucleus, Chiasm_CB should contain relatively more reads mapping to introns than Chiasm_PC. Indeed, Chiasm_CB contained, on average, 3% of reads mapping to introns versus 1.3% in Chiasm_PC (Fig. 4I).

To confirm that non-nucleated cell fragments are generated during our cell dissociation protocol, we dissociated the optic lobes of flies expressing membrane-bound GFP in chiasm glia following the same protocol used to generate the larva scRNA-seq dataset (Konstantinides et al. 2022). We observed similar-sized cell fragments of chiasm glia that contained (Fig. S5C) or did not contain (Fig. S5D) nuclei stained with Hoechst.

- Thirdly, we sought to investigate if cell fragmentation could explain the large discrepancy in the much higher proportion of cortex glia than expected. By nuclear counting using an anti-Repo antibody, we estimate that cortex glia represents less than 7% of all glia in the larval optic lobe (about 100 cortex glia out of about 1500 glia per optic lobe). However, they comprised the largest cluster in the larval dataset - about 43% of all optic lobe glial cells (1332 out of 3117 cells – after excluding central brain glia) (Fig. 2A and Fig. S5A-B). Like for chiasm glia, cortex glia clusters could be separated into cell body (Cortex_CB) and processes (Cortex_PC). Both clusters were transcriptionally similar (Fig. S5B), but Cortex_CB contained many more UMI, reads encoding TFs, and contained higher amount of *repo* mRNA than Cortex_PC (Fig. 4J-N). Cortex glia are very large cells that have processes around the somas of all cells, including neurons, neuroblasts, and the neuroepithelium (Fig. 4C), and might be broken into multiple fragments by the cell dissociation protocols used to generate scRNA-seq datasets. This likely explains the high number of Cortex_PC found in the dataset (41% of all glial “cells” in the L3 dataset – 1270 out of 3117 cells) compared to Cortex_CB (2% - 62 out of 3117 cells). Cortex_PC expressed higher levels of *fabp* (Fig. 4M) and *FK506-bp2* (Fig. 4N) than the Cortex_CB cluster. *Fabp* is a fatty acid binding protein whose mouse ortholog *Fabp7* mRNA is localized to the tripartite synapses in astrocytes and coimmunoprecipitates with the cytoplasmic polyadenylation element-binding 1 (CPEB1), which is responsible for regulating subcellular mRNA trafficking and translation inside cells (Gerstner et al. 2012; Huang et al. 2003). *FK506-bp2* was also enriched in Chiasm_PC, among other genes (Table S2). In conclusion, sequencing cellular processes without nuclei appears to explain the large discrepancy in the number of cortex glia cells in the dataset.

Finally, we sought to determine whether there was indeed a differential subcellular distribution of RNAs in chiasm glia *in vivo*. We identified *CG14598* as a gene that is highly and specifically expressed in both clusters of chiasm glia but not significant enriched in cell bodies or processes (Fig. S2A) (Fig. 4O). We performed HCR RNA-FISH for *repo* (Chiasm_CB only) and *CG14598* (Chiasm_CB and Chiasm_PC) in a fly line expressing membrane-bound GFP in chiasm glia (Fig. 4P). *repo* mRNA was only found around the nucleus in the cell body (Fig. 4P'), while *CG14598* mRNA was found throughout the cell (Fig. 4P''-P'''), which is consistent with the Chiasm_CB cluster being the cell body and Chiasm_PC the cell processes.

Taken together, these results show that when large cells such as glia are dissociated with commonly used scRNA-seq protocols, pieces of cells form "pseudo cells". Such cell fragments can mistakenly be identified as distinct cells using classical scRNA-seq clustering algorithms. Together, this phenomenon explains the presence of retina wrapping glia, the third cluster of chiasm glia, and the overrepresentation of cortex glia in the larval dataset.

Computational approaches to detect cellular processes in scRNA-seq datasets

We aimed to comprehensively identify and eventually remove cellular processes from our datasets to build an accurate atlas of the developing optic lobe glial cells (Fig. S6A). Droplets containing cellular process fragments have significantly fewer mRNAs while exhibiting unambiguous transcriptomic similarity to the clusters annotated as their corresponding cell body. They are also relatively deprived of transcription factor-encoding transcripts. Therefore, a more robust dataset can be analyzed by identifying and excluding cellular processes, the source of overrepresentation of some glia, and of extra clusters in the datasets.

We used two approaches to identify potential cellular process-containing clusters. These clusters contain lower total UMIs and lower transcription factor-encoding reads when compared to either the whole dataset (approach 1) or to the most similar cluster with high UMIs based on Pearson correlation (approach 2) (Fig. S6A).

Using both approaches for the larval dataset, we confirmed the previously identified clusters of chiasm and cortex glia that were investigated above as being cellular processes (Fig. S6B). Moreover, approach 1 also detected retina wrapping as processes and a newly identified cluster of processes of subperineurial cells. However, because these clusters were the only ones of their identity, they were not removed from the dataset. Moreover, both approaches identified two transcriptionally similar clusters of perineurial glia, one of them likely being the cellular processes of the other. Similarly to retina wrapping, chiasm and cortex, perineurial glia contain numerous cellular processes that extend around the whole optic lobe (Hartenstein 2011). In summary, for the larval

dataset, we excluded clusters comprised of cellular processes for chiasm, cortex, and perineurial glia.

Different from the larval dataset where cell types were already subdivided into multiple clusters, the adult dataset had most of its cell types as unique clusters; therefore, to better understand the possible presence of cellular process clusters in the adult dataset, we used both approaches and over-clustered the dataset into smaller subclusters (Fig. S6C-E). Both approaches showed that clusters Astrocytes_1, Astrocytes_2, and Astrocytes_4 were likely entirely comprised of cellular processes. Adult perineurial glia also could be divided into cell processes and cell bodies. The same was observed for cortex, distal satellite and medulla ensheathing glia. A subcluster of cluster Ensheathing_1 also showed up as processes in both approaches. Two subclusters of the Astrocytes_3 cluster were considered processes by approach 1, but were not excluded since, when compared to its closely correlated subclusters (approach 2), it did not show significant differences. In summary, we excluded 3 clusters of astrocytes-like glia, 1 cluster of cortex glia, 2 subclusters of perineurial glia, 1 subcluster of medulla ensheathing glia, 1 subcluster of ensheathing glia, and 1 subcluster of distal satellite glia (Fig. S6).

Taken together, these different approaches identified cellular processes that are the source of extra clusters in the dataset. This allowed us to build a more accurate atlas of the developing optic lobe glial cells in the larval (Fig. 5A-B) and adult stages (Fig. 5C-D) and assess the transcriptome of only the cell bodies (Table S1).

Discussion

Neuronal development highly depends on glial function (Fernandes et al. 2017; Kim et al. 2020; Poeck et al. 2001; Morante et al. 2013). To study glial development and diversity and its contributions to brain formation and function, it is essential to have access to their transcriptome throughout development. We comprehensively annotated all the optic lobe glial clusters from larva to adult stages using previously generated scRNA-seq datasets and collected marker genes information for each cluster (Table S1). Combined with our previous developmental scRNA-seq neuronal datasets (Özel et al. 2021), this provides a powerful tool to study neuron-glia interactions and glial development and function.

While Repo protein is a good marker for glial cells (Halter et al. 1995), its transcripts are lowly expressed and often not detected in glial clusters. *Repo* and *MRE16* long-noncoding RNA (aka CR34335) were previously proposed to be useful in identifying glial clusters (Davie et al. 2018). While if *repo* is often lowly expressed, it is only in glial cells. In contrast, *MRE16* is not specific to glial cells and is not a reliable marker, as observed for a VNC dataset that used both *repo* and *MRE16* and could not confidentially annotate all glial clusters based on these markers (Allen et al. 2020). Therefore, we found additional

markers that will be useful for broadly detecting glial scRNA-seq clusters in *Drosophila*: CG32032, AnxB9, and GstE12. Together with, or independently of *repo*, these markers identified all optic lobe glial clusters in larvae and adults.

After annotating the glial clusters in larva and adult, we investigated their transcriptional changes and increased diversity by integrating larvae, pupa, and adult stages. Retina wrapping glia change their functional type from nerve-wrapping in the larval retina to cortex glia in adults (Fig. 3). Retina wrapping glia coordinate neuronal differentiation and axon guidance during larval stages (Fernandes et al. 2017; Chang et al. 2018), and also serve to protect neurons crossing from one neuropil to another. However, because the retina touches the lamina in adults, there is no need for wrapping glia around photoreceptor axons between the retina and the lamina. We speculate that these glia do not die and are repurposed to serve as cortex glia (distal satellite). Other cells like inner and outer chiasm also formed a trajectory between the different stages, gradually changing from larval through the pupal stages to acquire their final fate in adult. However, these glia do not change their type, and their transcriptional changes are likely due to maturation.

However, some cells like cortex and perineurial glia do not form a trajectory between the different stages. This is expected since cortex and perineurial glia are generated before the beginning of optic lobe differentiation and are therefore already specified and mature when the larval cells were sequenced.

In contrast, there are cell types, such as lamina and medulla neuropil glia, that initially follow a single trajectory and then split into two (or more) branches during pupal stages to achieve different fates in adults (Fig. 3). An interesting example of this trajectory are medulla neuropil glia. After giving rise to different medulla neurons, the last division of medulla neuroblasts produces glial cells (Holguera and Desplan 2018; Li et al. 2013). These glia migrate towards the neuropil, passing over all neuronal somas and ending up with their cell bodies closest to the neuropil (Richier et al. 2017). At this larval stage, medulla neuropil glia do not seem to have acquired a terminal fate. Our data show that these medulla neuropil glia were transcriptionally indistinguishable from each other at larval stages. However, they start exhibiting differential gene expression after P30 before differentiating into at least two subtypes: astrocyte-like and ensheathing glia. Three hypotheses might explain how their final fate is determined: 1) the fate was determined at birth with undetectable transcriptional differences; 2) the fate was influenced by external cues depending on their final location in the neuropil; 3) cell fate was stochastically determined later. Interestingly, in mice, different states of microglia are determined by external cues in the neocortex; the cortical layer where these microglia end up residing in dictates their state based on the pyramidal neurons around them (Stogsdill et al. 2022). Similarly, lamina neuropil glia (epithelial and marginal) appear transcriptionally identical at early stages of development, only showing clearly separated

clusters around P30 (Fig. 3). A previous live-imaging study of these glia in larvae showed that, after migrating to the lamina, they interchange their position, sometimes occupying the epithelial glia layer, sometimes occupying the marginal glia layer (Bostock et al. 2020). Based on this evidence and our transcriptomic data, we hypothesize that for both medulla and lamina, neuropil glia are determined based on their final location, rather than an initial determination.

The lobula complex neuropil glia is another type of glia that we identified and validated in the larval dataset (Fig. S2). To our knowledge, the origin of these neuropil glia still remains to be elucidated. However, we hypothesize they originate from the central brain because the closest glia associated with them in our hierarchical clustering in larvae were chiasm glia (Fig. 2B) that originate from central brain neuroblasts (Viktorin et al. 2013). Moreover, they share common markers with the central brain glia validated in this study (Fig. S2). The central brain develops earlier than the optic lobe, and thus has mature astrocyte-like glia in larvae (Omoto et al. 2015; Kato et al. 2020). These glia are physically close to the lobula complex (Kato et al. 2020), which could explain the mature astrocyte-like glia in the lobula complex in the larva. In summary, our data suggest that larval lobula complex neuropil glia are mature astrocyte-like glia from the central brain that differentiated before cells were sequenced in our larval dataset.

We could also find additional lobula and lobula plate neuropil glia. These are named unknown neuropil glia (Astrocytes_3, Ensheathing_1 and Ensheathing_2). Because we could validate clusters for medulla and lamina neuropil glia, we speculate that, by elimination, the remaining clusters are lobula and lobula plate neuropil glia, which are the only remaining glia to be annotated in the optic lobe. Moreover, a recent scRNA-seq dataset using memory cassette for genes expressed in medulla precursor cells found glial cells corresponding to the clusters we identified as medulla astrocyte-like and medulla ensheathing glia, but not Astrocytes_3, nor Ensheathing_1 and _2 (Felix Simon, unpublished), suggesting that the cells of these clusters do not originate from medulla precursors, therefore strengthening our idea that such neuropil clusters may correspond to lobula and lobula plate neuropil glia.

Finally, we showed here that during cell dissociation, cells are fragmented into pieces that contain the nucleus (cell body) or not (processes). The cellular process fragments still hold enough RNA to be sequenced as unique cells and to pass through the quality control steps. Interestingly, the relatively fewer molecules of RNAs in processes are still sufficient to allow them to cluster with or next to their cell bodies. We devised approaches to identify cell process clusters by comparing the UMIs and transcription factor mRNAs within a cluster against the whole dataset or against their cell body counterpart. This allowed us to eliminate cell processes and produced a more accurate glial atlas of the larval and adult stages optic lobe (Fig. 5). However, instead of eliminating the processes, identifying them in the dataset can become a powerful tool to study subcellular localization

of mRNAs, especially for cells that are hard to isolate and to physically separate the cellular compartments. Therefore, we are working on a method that can discriminate processes and cell bodies in scRNA-seq datasets for any organism in both glia and neurons.

Methods

Drosophila strains

Flies were kept at 25 ºC 12-hour light/dark cycles on a standard cornmeal medium. 10xUAS-myr::GFP (BDSC #32197), UAS-RedStinger (#8546), Tret1-1-Gal4 (#67471), Vmat-Gal4 (#66806), rost::LacZ (#12042), CG3036::GFP (#50804), b-Gal4 (#76724), DAT-Gal4 (#84622), CG31663-Gal4 (#76708), ome-Gal4 (#76166), Canton-S (#64349), Hand-Gal4 (#66795), CG4288-Gal4::GFP (#29208), alphaTub85E::GFP (#60267), Npc2b-Gal4::GFP (#24694), Adgf-D-Gal4 (#77799), R25A01-Gal4 (#49102), UAS-CD8:GFP (from Bloomington), Cyp4g15-Gal4 (#39103), GstT4-Gal4 (#77777), nkd::LacZ (#25111), R94A08-Gal4 (#40673), UAS-GFP.nls (#4776), UAS-sfGFPnlsPEST-2A-B2ase – this is an unpublished line developed by Dr. Benjamin Choi (Desplan lab), consisting of a destabilized nuclear-localized GFP (Table Fly Genotypes).

Immunohistochemistry

Fly brains from adult stage or larva were dissected in room temperature 1x PBS. Then fixed in 4% formaldehyde (v/w) in 1x PBS for 20 minutes at room temperature. Following the fixation, the formaldehyde solution was removed and the brains were washed 3x in PBSTX (0.5% Triton X-100 in 1x PBS). Then, the brains were blocked in block solution (PBSTX with 5% Horse Serum) for at least 30 minutes at room temperature. Primary antibody was diluted as specified in block solution and the samples were incubated for two days at 4 ºC with primary antibody. Then the primary antibody solution was removed, and the brains were rinsed 3x with PBSTX and 1x washed with PBSTX for at least 2 hours. Then secondary antibodies were diluted in the block solution and added to the samples, which were incubated for two days at 4 ºC. Then, the samples were washed 2x with PBSTX and 1x with 1x PBS. Slides were mounted using a 0.22 mm spacer and samples immerged in Slowfade. Images were acquired in a Leica SP8 confocal. Images were processed in Fiji and Illustrator. The antibodies used are listed in (Table – antibodies).

HCR-RNA FISH

To perform fluorescence in situ hybridization (FISH) for the detection of RNAs, we used custom probes designed for *Repo, CG14598, and Cpr51A*. All probes were designed by Molecular Instruments (Choi et al. 2018). Hybridization buffer, amplification buffer, wash buffer, and fluorophore-labelled amplification hairpins (Alexa 546, 647, 594, and 488) were obtained from Molecular Instruments. We followed steps and reagents in the published protocol (Ferreira, A. A. G., Sieriebriennikov, B. & Whitbeck 2021). For combining HCR-RNA FISH and Immunohistochemistry, we performed the Immunohistochemistry first but using Molecular Instrument's Antibody Buffer instead of

PBSTX. Then fixed the tissue again in 4% PFA in PBST for 20 minutes at room temperature and then performed the HCR-RNA FISH protocol.

Antibody generation

Polyclonal antibodies were generated by Genscript (https://www.genscript.com/). The protein sequences used for each immunization were as follows: AnxB9 (guinea pig), MSSAEYYPFKCTPTVYPADPFDPVEDAAILRKAMKGFGTDEKAIIEILARRGIVQRLEIAE AFKTSYGKDLISDLKSELGGKFEDVILALMTPLPQFYAQELHDAISGLGTDEEAIIEILCTL SNYGIKTIAQFYEQSFGKSLESDLKGDTSGHFKRLCVSLVQGNRDENQGVDEAAAIAD AQALHDAGEGQWGTDESTFNSILITRSYQQLRQIFLEYENLSGNDIEKAIKREFSGSVE KGFLAIVKCCKSKIDYFSERLHDSMAGMGTKDKTLIRIIVSRSEIDLGDIKEAFQNKYGKS LESWIKMSIKSLTYVAIFGLFWGSIAGTVVDQFGIYGGSPITTTERSNAELRCMNINPQN SVDLEQ; CG32032 (rabbit),
MMGLWYGSEIIVHSQDFPGTYEYDSCVIIHLTDATDQIRLSQANRGYGYGNQDYNRNQ NNYGRTTTTQSSYPDSDEYPLRSIQSQQKYLRLIWSERDNNLEYTFNYTTSAPGQWS NIGDQRGSLVTLNTYTQFTGTVQVVKAVNDHLVLTFCGNDVKSSIYTVVLTRNRLGLSL DELRSIRNLLSRRGLYTETIRKVCNGCGRLGGSLFALLALLLVVRLAWGRGQ; Optix (rabbit),
AFSAAQVEIVCKTLEDSGDIERLARFLWSLPVALPNMHEILNCEAVLRARAVVAYHVGN FRELYAIIENHKFTKASYGKLQAMWLEAHYIEAEKLRGRSLGPVDKYRVRKKFPLPPTI WDGEQKTHCFKERTRSLLREWYLQDPYPNPTKKRELAKATGLNPTQVGNWFKNRRQ R; Repo (rat),
MEHDSFDDPIFGEFGGGPLNPLGAKPLMPTTTAMHPVMLGSVHELCSQQQQQQQQQ RLPDCNTILPNGGGGGAGSGGAGGSPNYVTKLDFVNKMGCYSPSQKYEYISAPQKLV EHHHHHH

Glia isolation and annotation from scRNA-seq in the adult stage

Glial clusters were isolated from the previously published dataset (Özel et al. 2021). We subset the clusters that were annotated as glial clusters by the authors based on high transcriptome correlation of these clusters with the bulk transcriptome of repo-positive sorted cells and low correlation with that of elav-positive sorted cells (Özel et al. 2021). We subset the following clusters from the final annotations found in the whole optic lobe adult dataset: “G04”, “G08”, “G03”, “G09”, “G06”, “G/LQ3”, “G02”, “G05”, “G14ab”, “G/LQ1”, “G11”, “G/LQ4”, “G10”, “G07”, “G01”, “G/LQ2”, “G12”, “G13”, “G16/LQ”. Then, we analyzed subset data using Seurat package in R. Specifically, genes that exhibit variable expression in the subset were identified with FindVariableFeatures, and the data was scaled with ScaleData before principal component analysis (RunPCA). The first 20 principal components were used to embed cells in a UMAP space for visualization (RunUMAP(dims = 1:20)) and to construct a nearest neighbor graph (FindNeighbors).

Re-clustering of the subset was performed with FindClusters(resolution = 0.6). This split the adult glial cells into 21 clusters, which were annotated accordingly to Table 2. For figure S6, we ran FindClusters(resolution = 2). (Script 2_Glia_Adult).

Glia isolation and annotation from scRNA-seq in the L3

Glial clusters were isolated from a previously published dataset (https://github.com/NikosKonst/larva_scSeq2022/blob/main/1_preparation_of_larval_pupal_dataset.R - larvaOL.integrated150.rds) (Konstantinides et al. 2022). We subset the clusters that presented a high transcriptome correlation with the bulk transcriptome of repo-positive FACS sorted cells and low correlation with that of elav-positive FACS-sorted cells (Fig. S1A) (Özel et al. 2021) (Script 1b_Glia_Larva_Correlations). Then, genes that show variable expression in the subset were identified with FindVariableFeatures. Principal component analysis was performed on scaled data (ScaleData followed by RunPCA). The first 30 principal components were used to embed cells in a UMAP space (RunUMAP(dims = 1:30)) and to construct a nearest neighbor graph (FindNeighbors). The subset data was then re-clustered with a resolution of 0.8 (FindClusters(resolution = 0.8)). This split the L3 glial cells into 23 clusters, which were annotated accordingly to Table 1. (Script 1_Glia_Larva)

Glia annotation in adult and larva

Larval glia are less studied than neurons, and we, therefore, sought specific markers to annotate and validate the clusters based on immunohistochemistry and/or RNA-FISH (Fig. S2A). Subperineurial glia, exclusively expressed rost (Fig. S2B). Perineurial glia expressed svp but not rost (Fig. S2B). Satellite glia expressed Optix (Fig. S2C) but did not express Dll, while lamina neuropil glia expressed both Optix and Dll (S2C and D).

- Chiasm glia (aka giant glia) expressed CG14598 (Fig. 4P) and DAT, a dopamine transporter responsible for the uptake of dopamine from synaptic sites (Fig. S2E and Fig. 4P). However, chiasm glia can be divided anatomically into two glia subtypes: outer chiasm (xgo) and inner chiasm (xgi). We manually subset and re-analyzed the chiasm cluster in order to separate it into two unsupervised clusters. We obtained two clusters that differentially expressed hth and were able to identify the two clusters as being xgo (hth-low) and xgi (hth-high) (Fig. S2F).

- Medulla neuropil glia were originally identified in three different closely associated clusters that changed gene expression rapidly through time. This may be the consequence of these glia originating from neuroblasts after their neurogenesis window. They then migrate past all neuron cell bodies to contact the neuropil. We merged the three clusters of medulla neuropil glia into one that exhibited expression of Hand and Dll (Fig. S2D and G).

- Lobula complex neuropil glia were validated by the expression of CG4288 (Fig. S2I), Dll (Fig. S2D), and Cpr51A (Fig. S2H).

- Cortex glia expressed CG4288 (aka MFS9) (Fig. S2I), and Cyp4g15 (Fig. 4C). Optic lobe cortex glia could be distinguished from central-brain cortex glia that expressed Npc2b (Fig. S2K).

- Additionally, we validated another two clusters as glial cells originating from the central brain based on their expression of Adgf-D (Fig. S2L) and their high correlation with each other (Fig. S2B). These central-brain glial clusters, together with the cortex central brain cluster, were excluded from the present analysis that focuses on the optic lobe.

In the adult, we could rely more on known markers from the literature, for example, we could identify perineurial glia based on the expression of Tret1-1 (Fig. S2) (Konstantinides et al. 2018) and the expression of Vmat (DeSalvo et al. 2014), which is also expressed in fenestrated glia (Fig. S2) (Romero-Calderón et al. 2008); subperineurial glia, as well as in the larva, exclusively expresses rost (Fig. S2), while pseudocartridge glia share the same subperineurial type markers but do not express rost, being the subperineurial glia from the lamina. Chalice glia expressed CG3036 and Optix (Fig. S3). Distal satellite glia was validated by the expression of vvl and b but neither Optix nor CG31663 (Fig. S3), while proximal satellite glia expressed vvl, b, Optix, and CG31663 (Fig. S3). Cortex clusters were annotated based on the expression of wrapper (Konstantinides et al. 2018) and validation with CG31663 (Fig. S3). Both outer and inner chiasm expressed CG31663, while outer chiasm expressed DAT and inner chiasm expressed ome and GstT4 (Fig. S3). Both Epithelial and Marginal glia expresses Optix, these clusters were manually separated and compared to the transcriptome of FACSorted epithelial and marginal glia (Script 2b_Glia_Adult_Corr_Epi_Marg), then it was validated by epithelial expressing b and marginal expressing ome and GstT4 (Fig. S2). Neuropil glia (astrocytes-like and ensheathing) are harder to separate and annotate because it is difficult to find specific markers that are exclusively expressed in one cluster compared to the other. We found two clusters of ensheathing that we annotated as medulla ensheathing based on the expression of known ensheathing glia markers, such as CG9657 (Richier et al. 2017) (more markers in Table 2), these clusters expressed CG31663 (also around lobula/lobula plate), nkd, and ome (both only around medulla, not lobula/lobula plate), which we found expressed in some of the medulla neuropil glia but not all. The medulla astrocytes-like cluster we annotated based on known astrocytes-like genes expression, such as wun2 (Brunet Avalos et al. 2019; Huang et al. 2015; Croset et al. 2018), we annotated this cluster as medulla based on nkd (Fig. S3) and because our integration showed that this cluster has a common trajectory with that of medulla ensheathing glia (Fig. 3). Other neuropil glia we annotated as astrocyte-like or ensheathing based on the same known markers above, but we could not validate their

identity. Because we did not find lobula/lobula plate neuropil glia in our adult dataset and because these other glial types formed a different trajectory that of medulla neuropil, we speculate these other neuropil glia are lobula/lobula plate neuropil.

Glia integration larva, pupa and adult

We integrated our annotated larval glia and adult datasets with glial cells from P15, P30, P50 and P70 stages. We used all clusters that were considered to be glia by the authors (Özel et al. 2021): "198", "212", "210", "201", "197", "207", "203", "196", "213", "219", "204", "200", "202", "185", "186", "187", "188", "189", "190", "199", "205", "206", "208", "209", "211", "216", "217". However, in the P15 stage, there was a cluster label as being of identity “206”, which was clustering by itself after integration, with no cell from other stages clustering together. Based on our analysis using the genes found in this paper as glial markers (*repo*, *CG32032*, *GstE12* and *AnxB9*), the cluster “206” in P15 is indeed not a glial cluster, we excluded this cluster from integration. After integrating all stages, we had a cluster in the center of the UMAP which was composed of cell from many different clusters and also expressed some neuronal markers (eg. brp, syt1), we excluded this cluster (Script 3_All_Glia_Integration).

We subset medulla neuropil (Fig. 3D-E) and the unknown neuropil (Fig. S4A-B) from the dataset with all stages. We used these clusters representing the early trajectory to look for early neuropil differentiation genes (Fig. S4C-H).

To look for common markers for early medulla and lamina neuropil glia, we used the integrated data and selected the clusters representing the beginning of the trajectory, and used the Seurat function FindMarkers (logfc.threshold = 1, min.diff.pct = 0.4).

Identification of Processes

We used two approaches based on a comparison of UMI and TFs. Approach 1 compared each cluster (or subcluster after over-clustering adult glia) with the whole dataset. To be considered processes, a cluster/ subcluster must have significantly fewer UMIs than the dataset (t-test p.adjusted < 0.005) and significantly fewer reads mapping to TFs than the dataset (t-test p.adjusted < 0.005). For approach 2, we compared each cluster/ subcluster with another cluster/ subcluster. To be considered processes, a cluster / subcluster must have significantly fewer UMIs (t-test p.adjusted < 0.005) than another close related cluster / subcluster (Pearson Correlation based on 2000 variable genes in the dataset > 0.9). Additionally, this cluster/ subcluster must also have fewer reads mapping to TFs (t-test p.adjusted < 0.005) than the cluster/ subcluster that it is being compared to (Script Functions).

Besides the results described in the result section, we had four clusters that showed up as being processes of other clusters by our approach 2: Inner Chiasm (processes) -> Medulla Ensheathing (cell body), Chalice -> Perineurial_CB, Epithelial and Marginal ->

Cortex, and Ensheathing_2 -> Cortex glia. We considered these events false positives since, with the exception of Ensheathing_2, all these clusters were validated as having separated cell identities (Fig. S3), and cluster Ensheathing_2 had its own markers (Table S1). Interestingly, out of these five clusters, only inner chiasm glia was shown as processes also using approach 1.

Data Availability

All raw and processed transcriptome data for the larval dataset are available at the GEO under accession number GSE167266. All raw and processed transcriptome data for the adult and pupa stages are at the GEO under GSE142787.

Code Availability

All related scripts used in this manuscript are available on GitHub https://github.com/AmandaAGF/Glia_Subcell_2023.

Acknowledgements

We thank the members of the fly community; the Bloomington stock center for flies; B. Choi for unpublished fly lines; Simon F. for sharing the unpublished medulla origin of glial cell types; Y-C Chen, E. O. Mazzoni, N. C. Leite, N. Konstantinides, S. Córdoba, I. Holguera, M. N. Özel, B. Sieriebriennikov and all members of the Desplan lab for discussions and feedback on the manuscript. This work was supported by NIH EY13012. A.A.G.F. was partly supported by NYU's GSAS MacCracken Program, and a Fleur Strand Graduate Fellowship (Biology Dept. NYU).

Author contributions

A.A.G.F conceived the project. A.A.G.F. performed and analyzed all experiments, wrote the original draft and prepared the figures. C.D. edited the manuscript.

Figure 1

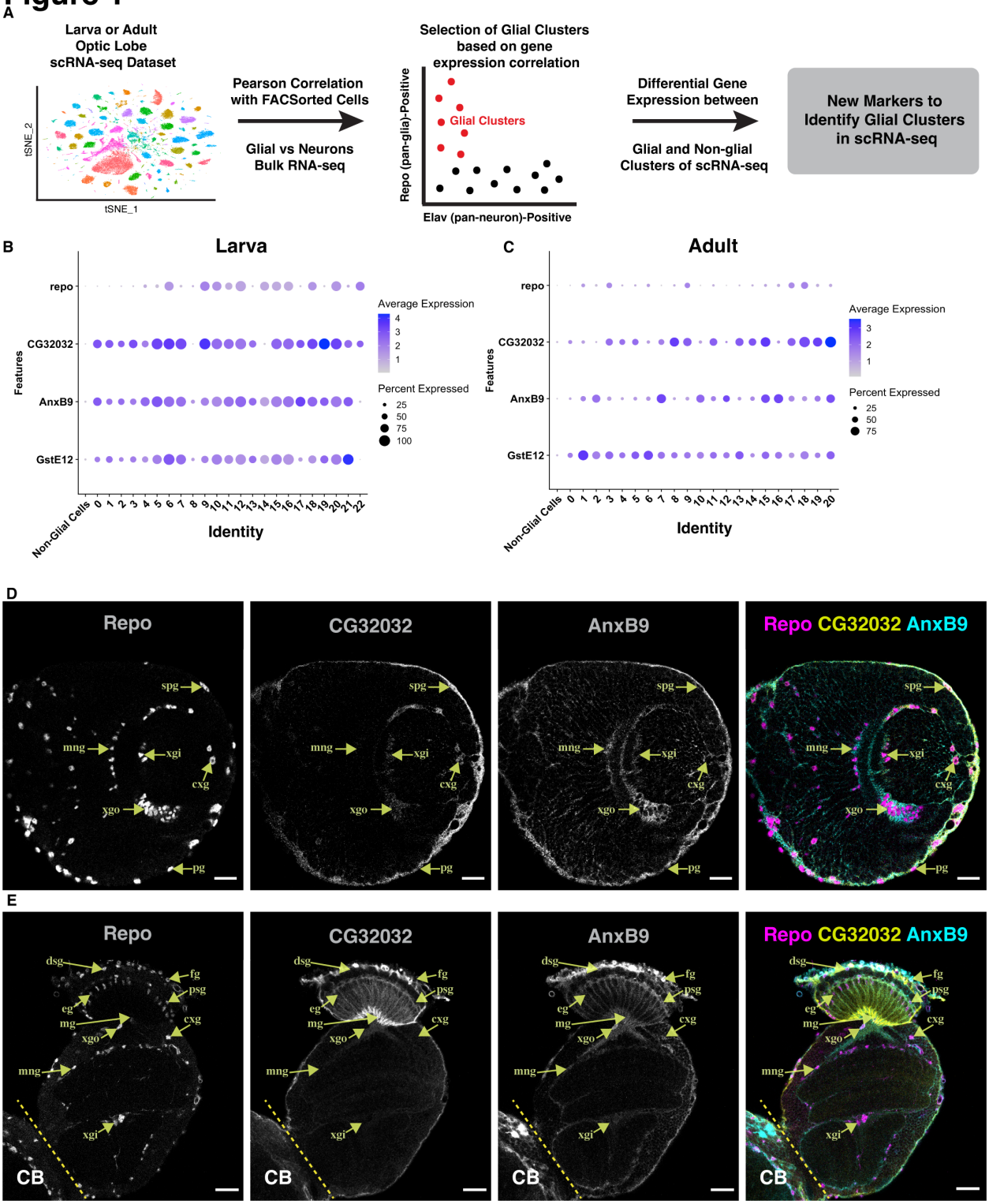

Figure 1. Identification of new glia-specific genes

(A) Schematic represention of how glial cell clusters were defined. Pearson correlation with the bulk transcriptome of Repo-positive and Elav-positive cells was used to

compare with the transcriptome of the clusters. The clusters defined as glia were used to find new glial markers.

(B) Dot Plot showing the expression of newly identified glial markers in larva (L3) cluster of glial cells or non-Glial Cells (Konstantinides 2022).

(C) Dot Plot showing the newly identified glial markers in adult clusters of glial or non-glial cells (Özel 2021).

(D) Immunostaining of larval (L3) optic lobes showing the overlap of Repo (pan-glia) CG32032, and AnxB9.

(E) Immunostaining of adult optic lobes showing the overlap of Repo (pan-glia) CG32032, and AnxB9. CB = Central Brain.

fg = fenestrated glia, pg = perineurial glia, spg = subperineurial glia, dsg = distal satellite glia, psg = proximal satellite glia, eg = epithelial glia, mg = marginal glia, xgo = outer chiasm glia, xgi = inner chiasm glia, cxg = cortex glia, mng = medulla neuropil glia, rwg = retina wrapping glia. Scale bar = 20 μm

Figure 2

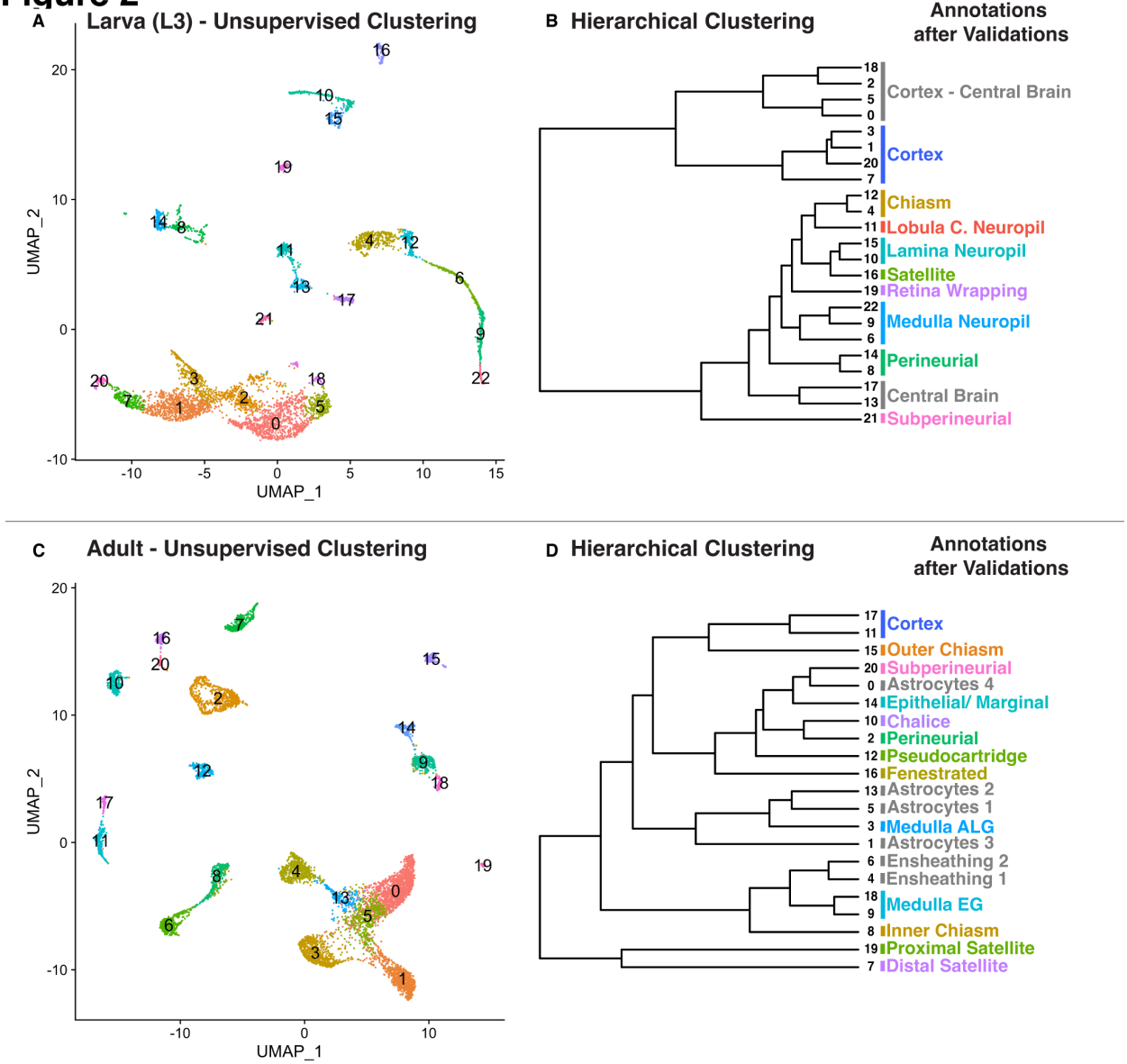

Figure 2. Annotation of glial clusters in a developmental scRNA-seq atlas of the fly optic lobe

- **(A)** Unsupervised clustering of larval glial cells reveals 23 clusters in an UMAP reduction.
- **(B)** The 23 clusters were organized by hierarchical clustering, which shows their transcriptional proximity to each cluster. The cluster identities correspond to the annotations after validations (Fig. S2).
- **(C)** Unsupervised clustering of adult glial cells reveals 21 clusters.
- **(D)** Hierarchical clustering and cluster identities after validations (Fig. S3).

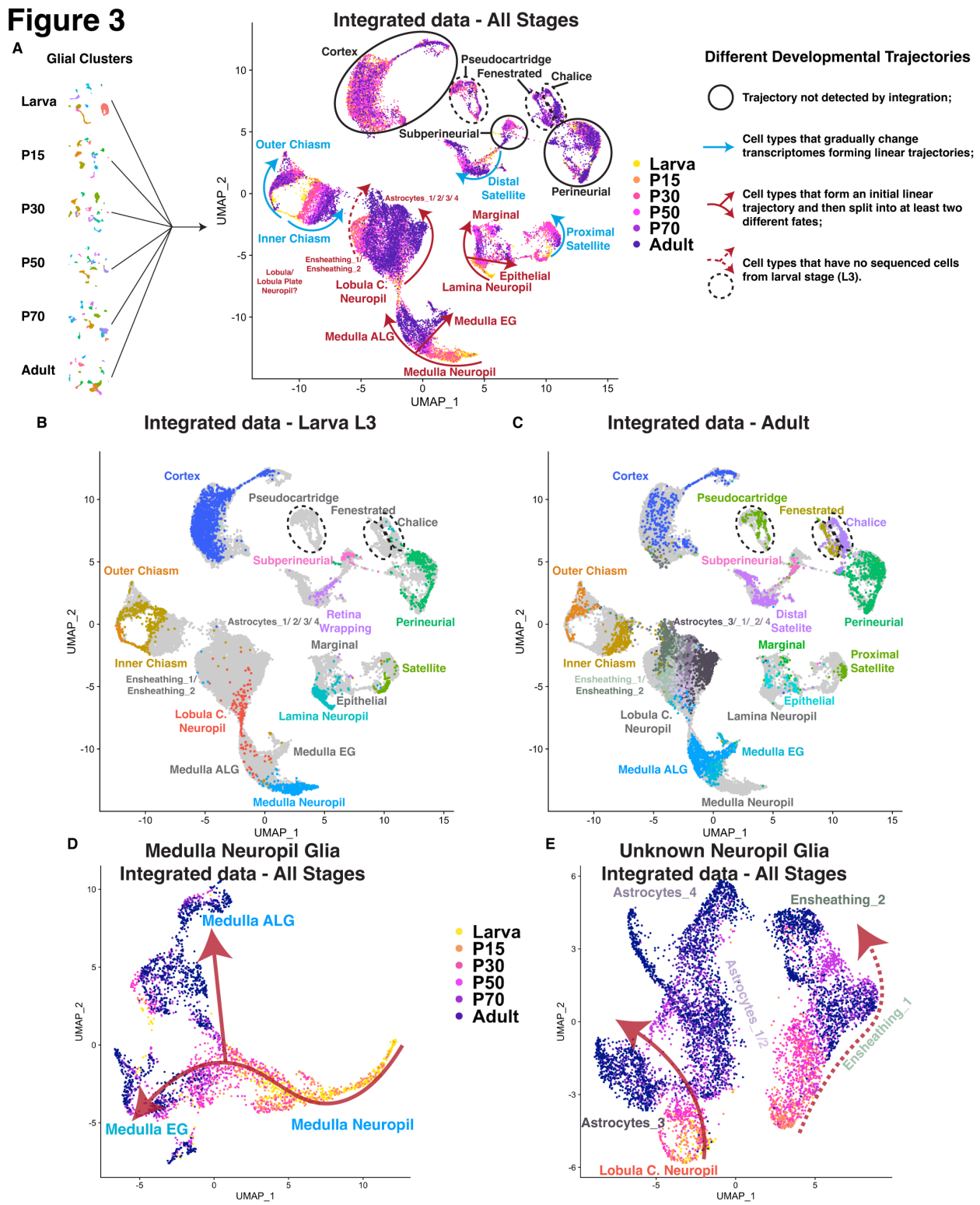

Figure 3. Developmental glial trajectories between larva and adult stages

(A-C) UMAP representing the integration of all glial cells from L3, P15, P30, P50, P70 and adult stages.

(A) Cells are colored according to their stage of origin. Blue arrows highlight glial cells that show a gradual developmental trajectory from L3 to adult in our integration. Red arrows are glial cells that are initially similar and progress to different terminal fates. Circled in black are highlighted glial cells that do not show a developmental trajectory from L3 to adult according to the integration. Dashed lines represent clusters that do not have cells from larva contributing to them.

(B) Only L3 cells are colored, and colors match glial clusters in Fig. 2B.

(C) Only adult cells are colored, and colors match glial clusters in Fig. 2D.

(D) UMAP represents only medulla neuropil glia isolated from the integrated dataset colored by stage.

(E) UMAP represents only the unknown neuropil glia (neither medulla nor lamina). They form two trajectories, one coming from Lobula C. Neuropil and giving rise to astrocytes-like glia, and the other starting from cells in P15 and giving rise to ensheathing glia. Colored by stage.

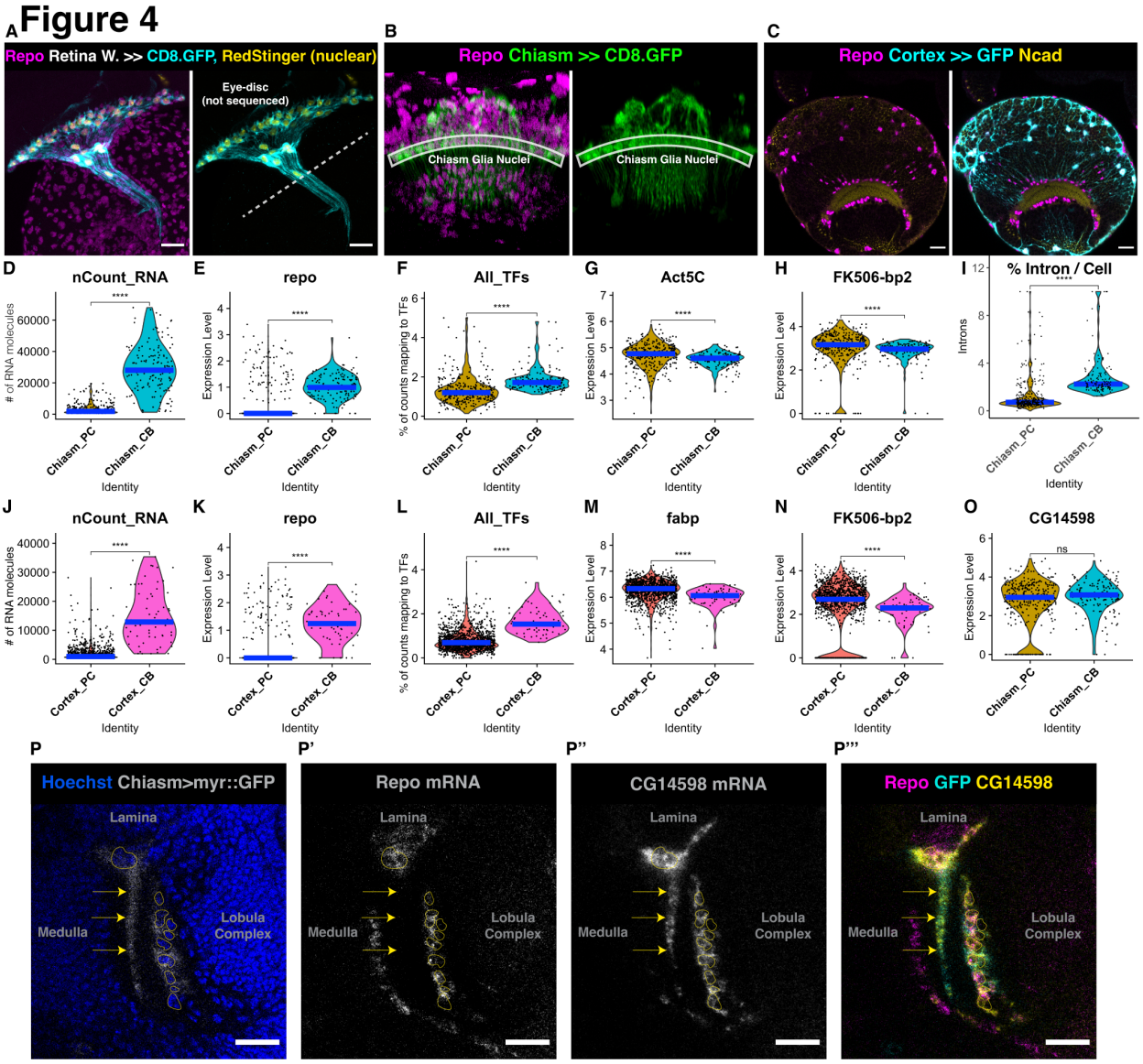

Figure 4. scRNA-seq reveals subcellular distribution of RNAs

(A) Retina Wrapping glia Gal4 driving expression of membrane-bound GFP (cyan) and RedStinger (nuclear) (yellow). Anti-Repo in the nuclei (magenta). The dashed line shows that the optic lobe and eye-disc were separated prior to sequencing of optic-lobe only.

(B) Chiasm glia Gal4 driving expression of membrane-bound GFP (green). Anti-Repo in the nuclei (magenta). White line around chiasm glia cell bodies.

(C) Cortex glia Gal4 driving expression of GFP (cyan). Anti-Repo in the nuclei (magenta) and Ncad shows neuropil (yellow).

(D-O) Violin plots comparing Chiasm_CB and Chiasm_PC (D-I and O) or Cortex_CB and Cortex_PC (J-N). Statistics by Wilcox-test, p-value < 0.00005 = ****, p-value > 0.05 = non-significant (ns). The blue bar represents the median.

(D) Number of UMIs per cell. Chiasm_CB had significantly more UMIs than Chiasm_PC.

(E) Expression level of *repo*. Chiasm_CB contains significantly more *repo* than Chiasm_PC.

(F) Percentage of reads that align to all transcription factors. Chiasm_CB have significantly more reads than Chiasm_PC.

(G) Expression level of *Act5C*. Chiasm_PC contains significantly more *Act5C* than Chiasm_CB.

(H) Expression level of *FK506-bp2*. Chiasm_PC contains significantly higher *FK506-bp2* than Chiasm_CB.

(I) Percentage of valid reads mapping to introns. Chiasm_CB has significantly more introns than Chiasm_PC.

(J) Number of UMIs per cell. Cortex_CB had significantly more UMIs than Cortex_PC.

(K) Expression level of *repo*. Cortex_CB contains significantly higher *repo* than Cortex_PC.

(L) Percentage of reads that align to all transcription factors. Cortex_CB have significantly more reads than Cortex_PC.

(M) Expression level of *fabp*. Cortex_PC contains significantly higher *fabp* than Cortex_CB.

(N) Expression level of *FK506-bp2*. Cortex_PC contains significantly higher *FK506-bp2* than Cortex_CB.

(O) Expression level of *CG14598*. Both clusters contained *CG14598* in similar levels.

(P) HCR RNA FISH of the L3 optic lobe expressing membrane-bound GFP in chiasm glia. Yellow lines highlight chiasm glia nuclei. Arrows point to chiasm glia processes. Hoechst shows nuclei of all cells in blue. DAT-Gal4 express membrane-bound GFP (grey) in chiasm glia to visualize chiasm glia membrane. We did not use any staining against GFP (neither immunostaining nor FISH). Scale bar = 20 μm.

(P') *Repo* mRNA is found around the nuclei, but not in the processes of chiasm glia.

(P'') *CG14598* mRNA is found around the nuclei and in the processes of chiasm glia.

(P''') Merged image, *repo* (magenta), GFP (cyan) and *CG14598* (yellow).

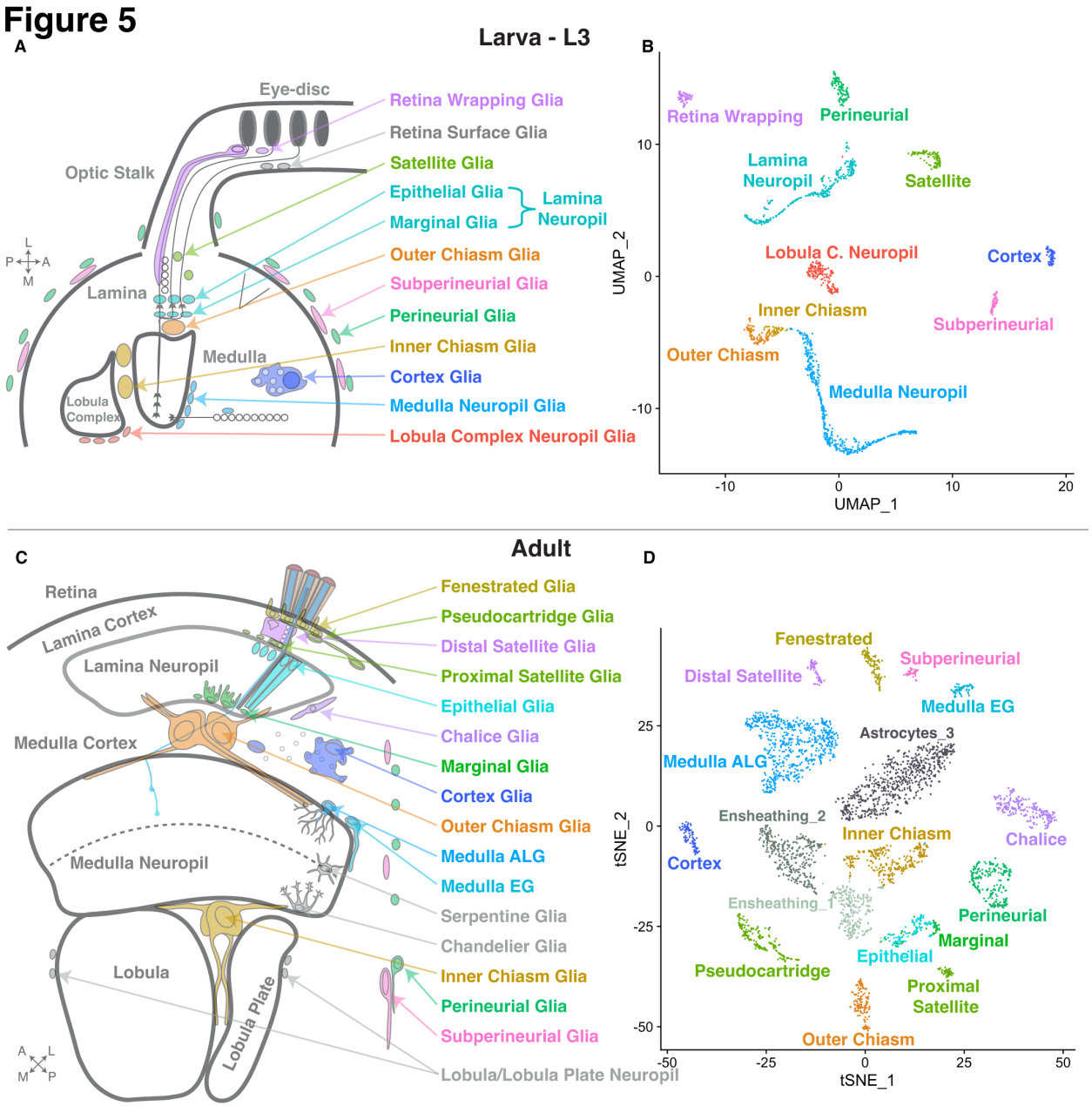

Figure 5. Final Annotation of glia in the developmental single-cell atlas of the optic lobe

(A) A cross-section schematic representation of the larva (L3) optic lobe with drawings of the glial cells.

(B) UMAP visualization of the final larval glial cells annotations after removal of cellular processes in the dataset (Table 1). Colors of the clusters match the color of the drawing in Fig A.

(C) A cross-section schematic representation of the adult stage optic lobe with drawings of the glial cells.

(D) TSNE visualization of the final adult stage glial cells annotations after removal of cellular processes in the dataset (Table 2). Colors of the clusters match the color of the drawing in Fig C.

Tables

Table 1: Larval glial clusters annotation.

Annotation from Konstantinides et al. 2022	Cluster #	Cluster Final Annotation	Cluster Annotation based on Literature	Cluster Annotation based on Validations	Gene Expressed in the Cluster	Reference	Obs
91	19	Retina Wrapping Glia	Retina Wrapping Glia	Retina Wrapping Glia	CG16857	1	Retina Wrapping Glia based on validation (Figure S2)
					alphaTub85E	2	
					alphaTub85E	Figure S2	
45	12	Outer Chiasm	Chiasm	Outer Chiasm	alrm	3	Chiasm Glia based on literature (alrm, wnt4), janelia line (wb). Manually separated into two clusters, one being Outer Chiasm based on validations (Figure S2) and Integration (Figure 3)
					Wnt4	4	
					wb	Janelia line R18E12	
					DAT	Figure S2	
					Hth-low	Figure S2	
					Cpr51A	Figure S2	
					CG14598	Figure 4	
45	12	Inner Chiasm	Chiasm	Inner Chiasm	alrm	3	Chiasm Glia based on literature (alrm, wnt4), janelia line (wb). Manually separated into two clusters, one being Inner Chiasm based on validations (Figure S2) and Integration (Figure 3)
					Wnt4	4	
					wb	Janelia line R18E12	
					DAT	Figure S2	
					Hth-high	Figure S2	
					Cpr51A	Figure S2	
					CG14598	Figure 4	
45	4	Chiasm_PC	Chiasm	Chiasm	alrm	3	Highly similar transcriptome to Outer and Inner Chiasm. But is a cluster composed of cellular processes of these cells. Discussed in section "scRNAseq reveals subcellular distribution of RNAs"
					Wnt4	4	
					wb	Janelia line R18E12	
					CG14598	Figure 4	
56	21	Subperineurial	Subperineurial	Subperineurial	moody	5	Subperineurial based on validation (Figure S2) and integration (Figure 3)
					Mdr65	5	
					rost	Figure S2	

56	8	Perineurial_PC	Perineurial	Perineurial	CG4797	6	Perineurial based on validation (Figure S2) and integration (Figure 3).
56	14	Perineurial_CB			MFS2	7	
					svp+ rost-	Figure S2	
63	10	Lamina Neuropil	Lamina Neuropil	Lamina Neuropil	bi	8	Lamina Neuropil based on validation (Figure S2) and integration (Figure 3). There are two clusters, which are early (10) vs late (15) Lamina Neuropil, since one expresses gcm (early glial marker).
63	15	Lamina Neuropil			Optix	9	
					loco	10	
					gcm	11	
					Optix	Figure S2	
					Dll	Figure S2	
87	16	Satellite	Satellite	Satellite	bi	8	Satellite based on validation (Figure S2) and integration (Figure 3)
					Optix+ Dll-	Figure S2	
44	22	Medulla Neuropil	Medulla Neuropil	Medulla Neuropil	gcm	11	Medulla neuropil glia were found in three cluster by unsupervised clustering. These glial cells are changing rapidly through time which could explain the cluster split. We confirmed that these clusters are highly similar transcriptionally compared to other clusters and express markers of mng, therefore they were merged into one cluster in L3. Mng based on validation (Figure S2) and integration (Figure 3).
					loco	13	
					Hand	Figure S2	
44	9	Medulla Neuropil	Medulla Neuropil	Medulla Neuropil	gcm	11	
					loco	13	
					Dll	14	
					Hand	Figure S2	
					Dll	Figure S2	
44	6	Medulla Neuropil	Medulla Neuropil	Medulla Neuropil	gcm	11	
					loco	13	
					Eaat1	4, 13	
					Dll	14	
					Dll	Figure S2	
2	1	Cortex_PC	Cortex	Cortex	wrapper	6	Cortex based on validations with CG4288 and Cyp4g15 (Figure S2 and Figure 4)
2	3	Cortex_PC			Cyp4g15	12	
2	7	Cortex_PC			Cyp4g15	Figure 4 C	
85	20	Cortex_CB			CG4288	Figure S2	
					Npc2b-	Figure S2	

3	0	Cortex Central Brain	Cortex	Cortex Central Brain	wrapper	6	Cortex based on validation with CG4288, from central brain based on Npc2b (Figure S2)
3	2	Cortex Central Brain			Cyp4g15	12	
3	5	Cortex Central Brain			CG4288	Figure S2	
85	18	Cortex Central Brain			Npc2b+	Figure S2	
67	11	Lobula Complex Neuropil	Neuropil - Astrocytes-Like	Lobula Complex Neuropil	Gs2	6	Lobula Complex Glia based on validations (Figure S2)
					Eaat1	4, 13	
					Cpr51A	Figure S2	
					CG4288	Figure S2	
					Dll	Figure S2	
67	13	Central Brain		Central Brain	Adgf-D	Figure S2	Only one cluster expresses Adgf-D, however, both clusters are very similar transcriptionally (Figure 3.3 B - Hierarchical clustering) and also expresses some of the markers we see in central brain and lobula complex glia, for example CG4288. But not express Cpr51A (only Lobula Complex). Therefore, we considered both cluster as coming from Central Brain.
67	17	Central Brain					

Table with all the clusters annotations for larval glial cells. References: (Cameron et al. 2016) (1). (Matthews et al. 1990) (2). (Nakano et al. 2019) (3). (Edwards et al. 2012) (4). (DeSalvo et al. 2014) (5). (Konstantinides et al. 2018) (6). (McMullen et al. 2021) (7). (Hofmeyer et al. 2008) (8). (Chen et al. 2016) (9). (Chotard and Salecker 2007) (10). (Chotard et al. 2005) (11). (Spéder and Brand 2018) (12). (Richier et al. 2017) (13). (Konstantinides et al. 2022) (14).

Table 2: Adult glial clusters annotation.

Annotation from Ozel et al. 2021	Cluster #	Cluster Final Annotation	Cluster Annotation based on Literature	Cluster Annotation based on Validations	Gene Expressed in the Cluster	Reference	Obs
G/LQ1 186	5	Astrocytes_1	Astrocytes-Like		Eaat1	1	
					wun2	2,3,4	
G/LQ1 186	13	Astrocytes_2	Astrocytes-Like		Tsp5D	2	
					CG1732	2	
					Eaat1	1	
					CG7607	3	
					CG15209	1,3	
					CG1537	3,4	
					wun2	2,3,4	
G10 205	1	Astrocytes_3	Astrocytes-Like		Act79B	1	Astrocytes-like accordingly to the literature
					CG34367	3	
					flw	4,5	
					e	1	
					GstD3	3	
					CG13631	1	
					CG1537	3,4	
					wun2	2,3,4	
G02 187	3	Astrocytes_ALG	Astrocytes-Like	Medulla_ALG	CG42342	4,5	Medulla neuropil glia based on integration (Figure 3) and validation (Figure S3). Astrocyte-like based on genes expressed and literature.
					CG1732	2	
					CG31705	1,2,4,5	
					ogre	1	
					wun2	2,3,4	
					htl	6	
					nkd	Figure S3	
G13 208	2	Perineurial	Perineurial	Perineurial	CG4797	1	Perineurial based on validations (Figure S3) and integration (Figure 3)
					CG3168	1	
					Tret1-1	1	
					CG14687	1	
					Tret1-1	Figure S3	
					Vmat	Figure S3	

G/LQ4 197	4	Ensheathing_1	Ensheathing		CG9657	6	Ensheathing accordingly to the literature.
					Ugt35b	1	
					CG16743	1	
					CG8369	1	
					CG3940	1	
					FaS3	5	
					CG14945	5	
					zyd	4,5	
G01 185	6	Ensheathing_2	Surface/ Ensheathing		CG6287	2	Based on literature could be surface or ensheathing. Based on hierarchical clustering, it is closer to Ensheathing glia. It has its own combination of markers (Supplementary Table 1)
					CG9436	2	
					CG9657	6	
					CG8369	1	
G07 202	7	Distal Satellite Glia	Chiasm	Distal Satellite	CG4716	5	Distal Satellite based on validations (Figure S3) and integration (Figure 3)
					CG15201	1	
					hoe1	1	
					vvl+ Optix-	Figure S3	
					b	Figure S3	
G/LQ3 196	8	Inner_Chiasm	Ensheathing	Inner Chiasm	CG9657	6	Inner Chiasm based on validation (Figure S3) and integration (Figure 3)
					CG7509	1	
					Ugt35b	1,4	
					CG8369	1	
					FaS3	4	
					ome	Figure S3	
					CG31663	Figure S3	
G03 198	9	Medulla_EG_1	Ensheathing	Medulla Ensheathing	CG9657	6	Medulla neuropil glia based on validation (Figure S3) and integration (Figure 3).
G04 199	18	Medulla_EG_2		Medulla Ensheathing	CG16743	1	
					CG3940	1	
					axo	1,5	

					CG4829	4,5	Ensheathing based on genes expressed and literature. We found two clusters of Medulla Ensheathing.
					drpr	1	
					CG31663	Figure S3	
					nkd	Figure S3	
					ome	Figure S3	
G12 207	10	Chalice	Surface	Chalice	CG3036	7	Chalice based on validation (Figure S3)
					CG10444	7	
					Optix	Figure S3	
					CG3036	Figure S3	
G05 200	11	Cortex_1	Cortex	Cortex	wrapper	1	Cortex based on validation (Figure S3) and integration (Figure 3).
G06 201	17	Cortex_2		Cortex	wtrw	1	
					CG3270	5	
					Ddc	5	
					CG31663	Figure S3	
G14ab 188	14	Epithelial		Epithelial	Optix	Figure S3	This cluster was manually separated into two (Methods) and compared to the transcriptome of FACS sorted epithelial and marginal glia (ref 10). Based on higher correlation, G14a (212 in pupa) is Epithelial and G14b (213 in pupa) is Marginal. Validation using specific markers (Figure S3)
					b+	Figure S3	
					GstT4-	Figure S3	
G14ab 188	14	Marginal		Marginal	ome	Figure S3	
					Optix	Figure S3	
					b-	Figure S3	
					GstT4+	Figure S3	
G16/LQ 189	12	Pseudocartridge	Subperineurial	Pseudocartridge	glob1	1	Expresses markers of subperineurial glia type, but do not express the marker rost, which was found only in subperineurial around medulla, lobula and lobula plate.
					CG9512	1	
					Cat	1	
					CG11413	5	
					bond	1	

G08 203	15	Outer_Chiasm	Chiasm		Irk3	1	Outer Chiams based on validation (Figure S3) and integration (Figure 3)
					CG15201	1	
					CG4288	2	
					CG31690	5	
					CG31663	Figure S3	
					DAT	Figure S3	
G11 206	16	Fenestrated	Fenestrated	Fenestrated	Vmat	9	Fenestrated based on validation (Figure S3)
					Vmat+ Tret-1-	Figure S3	
G11 206	20	Subperineurial	Subperineurial	Subperineurial	Mdr65	7	Subperineurial based on validation (Figure S3) and integration (Figure 3)
					moody	7	
					Gli	7	
					CG18067	5	
					rost	Figure S3	
G09 204	19	Proximal Satellite	Cortex	Proximal Satellite	CG12269	5	Proximal Satellite based on validations (Figure S3) and integration (Figure 3)
					Npc2a	2	
					CG12269	4,5	
					CG9686	1,2	
					wtrw	1	
					vvl+ Optix+	Figure S3	
					b	Figure S3	
					CG31663	Figure S3	
G/LQ2 190	0	Astrocytes_4	Astrocytes-like		wun2	2,3,4	

Table with all the clusters annotations for adult glial cells. References: (Konstantinides et al. 2018) (1). (Brunet Avalos et al. 2019) (2). (Huang et al. 2015) (3). (Croset et al. 2018) (4). (Davie et al. 2018) (5). (Richier et al. 2017) (6). (DeSalvo et al. 2014) (7). (Romero-Calderón et al. 2008) (9). (Davis et al. 2020) (10).

Table 3: Early markers of neuropil glia

Gene	p_val	avg_log2FC	pct.1	pct.2	p_val_adj
pyd	0	1.27741953	0.913	0.225	0
CG8507	0	1.216948511	0.861	0.269	0
l(3)neo38	0	1.293375905	0.869	0.254	0
CG11670	0	2.39173408	0.48	0.003	0
sqd	0	1.549881948	0.97	0.407	0
cv-c	0	1.516949612	0.752	0.098	0
Set	0	1.011634961	0.857	0.278	0
FK506-bp1	0	1.127594639	0.656	0.128	0
repo	0	1.07129291	0.834	0.241	0
hdly	0	1.28066888	0.63	0.196	0
r-l	0	1.096643793	0.458	0.044	0
pnt	0	1.722796657	0.894	0.171	0
E(spl)mdelta-HLH	0	1.427573876	0.528	0.054	0
E(spl)mgamma-HLH	0	2.744625903	0.474	0.04	0
E(spl)mbeta-HLH	0	1.381859984	0.952	0.409	0
E(spl)malpha-BFM	0	2.065636247	0.531	0.068	0
E(spl)m2-BFM	0	1.114562998	0.544	0.089	0
E(spl)m3-HLH	0	2.26475747	0.956	0.316	0
E(spl)m7-HLH	0	3.099438691	0.894	0.144	0
His2Av	0	1.587817193	0.939	0.304	0
CG7911	0	1.069325256	0.807	0.237	0
Nlp	0	1.309119297	0.949	0.394	0
hdc	0	1.875775676	0.966	0.29	0
klar	0	1.26847359	0.724	0.11	0
Tet	0	1.134444502	0.876	0.302	0
Tsp68C	0	1.074969418	0.637	0.093	0
CG9705	0	1.016699832	0.688	0.153	0
Pep	0	1.003769878	0.881	0.3	0
CR30009	0	3.725538098	0.742	0.055	0
SmD3	0	1.119441223	0.811	0.198	0
shot	0	1.14116922	0.754	0.164	0
CG14478	0	1.005887976	0.685	0.149	0
Glycogenin	0	1.538628816	0.611	0.13	0
HmgD	0	1.581760542	0.954	0.405	0
babos	0	1.022883616	0.635	0.145	0
CG3800	0	1.489660242	0.955	0.394	0

Dll	0	1.016931551	0.575	0.111	0
br	0	1.233861977	0.496	0.055	0
N	0	1.196607123	0.971	0.375	0
pigs	0	1.028431913	0.517	0.087	0
CG43658	0	1.457990352	0.926	0.29	0
CG42684	0	1.122937002	0.812	0.179	0
CG6891	0	1.728238876	0.883	0.31	0
CG43759	0	1.014922267	0.534	0.085	0
Traf4	0	1.965196543	0.62	0.034	0
Lam	0	1.178054183	0.846	0.199	0
Ent2	0	1.020780603	0.822	0.209	0
smt3	0	1.226925998	0.985	0.571	0
gcm	0	3.675797829	0.608	0.017	0
gcm2	0	1.42091828	0.411	0.005	0
hoip	0	1.050552314	0.608	0.095	0
eEF1delta	0	1.230100215	0.905	0.288	0
dUTPase	0	1.315126316	0.649	0.117	0
crol	0	1.161981626	0.945	0.339	0
CadN	0	1.108181652	0.706	0.118	0
CG9336	0	2.347068703	0.696	0.169	0
Df31	0	1.478189972	0.982	0.571	0
hth	1.60E-302	1.188675551	0.665	0.239	2.14E-298
Gdh	1.25E-288	1.186730922	0.688	0.271	1.67E-284
Hs6st	7.81E-274	1.055446895	0.616	0.215	1.05E-269
emc	4.30E-273	1.131679898	0.926	0.456	5.77E-269

Table with the genes that are markers for medulla and lamina neuropil early trajectory.

Table S1: Markers glia larva and adult.

Table S2: Markers processes of chiasm and cortex glia in larva.

Table S3: Comparison of clusters from larva and adult after integration.

Supplementary information: Tables of fly genotypes and antibodies.

References

Allen AM, Neville MC, Birtles S, Croset V, Treiber CD, Waddell S, Goodwin SF. 2020. A single-cell transcriptomic atlas of the adult Drosophila ventral nerve cord. *Elife* **9**. https://elifesciences.org/articles/54074.

Bostock MP, Prasad AR, Chaouni R, Yuen AC, Sousa-Nunes R, Amoyel M, Fernandes VM. 2020. An Immobilization Technique for Long-Term Time-Lapse Imaging of Explanted Drosophila Tissues. *Front Cell Dev Biol* **8**. https://www.frontiersin.org/article/10.3389/fcell.2020.590094/full.

Brunet Avalos C, Maier GL, Bruggmann R, Sprecher SG. 2019. Single cell transcriptome atlas of the Drosophila larval brain. *Elife* **8**. https://elifesciences.org/articles/50354.

Cameron S, Chen Y, Rao Y. 2016. Borderless regulates glial extension and axon ensheathment. *Dev Biol* **414**: 170–180. https://linkinghub.elsevier.com/retrieve/pii/S0012160616302445.

Carson JH, Cui H, Barbarese E. 2001. The balance of power in RNA trafficking. *Curr Opin Neurobiol* **11**: 558–563. https://linkinghub.elsevier.com/retrieve/pii/S095943880000249X.

Chang Y-C, Tsao C-K, Sun YH. 2018. Temporal and spatial order of photoreceptor and glia projections into optic lobe in Drosophila. *Sci Rep* **8**: 12669. http://www.nature.com/articles/s41598-018-30415-8.

Chen Z, Del Valle Rodriguez A, Li X, Erclik T, Fernandes VM, Desplan C. 2016. A Unique Class of Neural Progenitors in the Drosophila Optic Lobe Generates Both Migrating Neurons and Glia. *Cell Rep* **15**: 774–786. https://linkinghub.elsevier.com/retrieve/pii/S2211124716303321.

Choi HMT, Schwarzkopf M, Fornace ME, Acharya A, Artavanis G, Stegmaier J, Cunha A, Pierce NA. 2018. Third-generation in situ hybridization chain reaction: multiplexed, quantitative, sensitive, versatile, robust. *Development* **145**. https://journals.biologists.com/dev/article/145/12/dev165753/48466/Third-generation-in-situ-hybridization-chain.

Chotard C, Leung W, Salecker I. 2005. glial cells missing and gcm2 Cell Autonomously Regulate Both Glial and Neuronal Development in the Visual System of Drosophila. *Neuron* **48**: 237–251. https://linkinghub.elsevier.com/retrieve/pii/S0896627305007865.

Chotard C, Salecker I. 2007. Glial cell development and function in the Drosophila visual system. *Neuron Glia Biol*.

Condeelis J, Singer RH. 2005. How and why does β-actin mRNA target? *Biol Cell* **97**: 97–110. http://doi.wiley.com/10.1042/BC20040063.

Croset V, Treiber CD, Waddell S. 2018. Cellular diversity in the Drosophila midbrain revealed by single-cell transcriptomics. *Elife* **7**. https://elifesciences.org/articles/34550.

D'Arcy BR, Silver DL. 2020. Local gene regulation in radial glia: Lessons from across the nervous system. *Traffic* **21**: 737–748. https://onlinelibrary.wiley.com/doi/10.1111/tra.12769.

Davie K, Janssens J, Koldere D, De Waegeneer M, Pech U, Kreft Ł, Aibar S, Makhzami

S, Christiaens V, Bravo González-Blas C, et al. 2018. A Single-Cell Transcriptome Atlas of the Aging Drosophila Brain. *Cell* **174**: 982-998.e20. https://linkinghub.elsevier.com/retrieve/pii/S0092867418307207.

Davis FP, Nern A, Picard S, Reiser MB, Rubin GM, Eddy SR, Henry GL. 2020. A genetic, genomic, and computational resource for exploring neural circuit function. *Elife* **9**. https://elifesciences.org/articles/50901.

DeSalvo MK, Hindle SJ, Rusan ZM, Orng S, Eddison M, Halliwill K, Bainton RJ. 2014. The Drosophila surface glia transcriptome: evolutionary conserved blood-brain barrier processes. *Front Neurosci* **8**. http://journal.frontiersin.org/article/10.3389/fnins.2014.00346/abstract.

Desalvo MK, Mayer N, Mayer F, Bainton RJ. 2011. Physiologic and anatomic characterization of the brain surface glia barrier of Drosophila. *Glia* **59**: 1322–1340. https://onlinelibrary.wiley.com/doi/10.1002/glia.21147.

Eberhard DA, Brown MD, VandenBerg SR. 1994. Alterations of annexin expression in pathological neuronal and glial reactions. Immunohistochemical localization of annexins I, II (p36 and p11 subunits), IV, and VI in the human hippocampus. *Am J Pathol* **145**: 640–9. http://www.ncbi.nlm.nih.gov/pubmed/8080046.

Edwards TN, Meinertzhagen IA. 2010. The functional organisation of glia in the adult brain of Drosophila and other insects. *Prog Neurobiol* **90**: 471–497. https://linkinghub.elsevier.com/retrieve/pii/S0301008210000122.

Edwards TN, Nuschke AC, Nern A, Meinertzhagen IA. 2012. Organization and metamorphosis of glia in the Drosophila visual system. *J Comp Neurol* **520**: 2067–85. http://www.ncbi.nlm.nih.gov/pubmed/22351615.

Fernandes VM, Chen Z, Rossi AM, Zipfel J, Desplan C. 2017. Glia relay differentiation cues to coordinate neuronal development in Drosophila. *Science (80-)*.

Ferreira, A. A. G., Sieriebriennikov, B. & Whitbeck H. 2021. HCR RNA-FISH protocol for the whole-mount brains of Drosophila and other insects. *Protocols.io*.

Freeman MR, Doherty J. 2006. Glial cell biology in Drosophila and vertebrates. *Trends Neurosci* **29**: 82–90. https://linkinghub.elsevier.com/retrieve/pii/S0166223605003073.

Gerstner JR, Vanderheyden WM, LaVaute T, Westmark CJ, Rouhana L, Pack AI, Wickens M, Landry CF. 2012. Time of Day Regulates Subcellular Trafficking, Tripartite Synaptic Localization, and Polyadenylation of the Astrocytic Fabp7 mRNA. *J Neurosci* **32**: 1383–1394. https://www.jneurosci.org/lookup/doi/10.1523/JNEUROSCI.3228-11.2012.

Halter DA, Urban J, Rickert C, Ner SS, Ito K, Travers AA, Technau GM. 1995. The homeobox gene repo is required for the differentiation and maintenance of glia function in the embryonic nervous system of Drosophila melanogaster. *Development* **121**: 317–332. https://journals.biologists.com/dev/article/121/2/317/38726/The-homeobox-gene-repo-is-required-for-the.

Hartenstein V. 2011. Morphological diversity and development of glia in Drosophila. *Glia* **59**: 1237–1252. https://onlinelibrary.wiley.com/doi/10.1002/glia.21162.

Herbert AL, Fu M, Drerup CM, Gray RS, Harty BL, Ackerman SD, O'Reilly-Pol T,

Johnson SL, Nechiporuk A V., Barres BA, et al. 2017. Dynein/dynactin is necessary for anterograde transport of Mbp mRNA in oligodendrocytes and for myelination in vivo. *Proc Natl Acad Sci* **114**. https://pnas.org/doi/full/10.1073/pnas.1711088114.

Ho MS, Verkhratsky A, Duan S, Parpura V. 2019. Editorial: Glia in Health and Disease. *Front Mol Neurosci* **12**. https://www.frontiersin.org/article/10.3389/fnmol.2019.00063/full.

Hofmeyer K, Kretzschmar D, Pflugfelder GO. 2008. Optomotor-blind expression in glial cells is required for correct axonal projection across the Drosophila inner optic chiasm. *Dev Biol* **315**: 28–41. https://linkinghub.elsevier.com/retrieve/pii/S0012160607014352.

Holguera I, Desplan C. 2018. Neuronal specification in space and time. *Science (80-)* **362**: 176–180. https://www.science.org/doi/10.1126/science.aas9435.

Huang Y-S, Carson JH, Barbarese E, Richter JD. 2003. Facilitation of dendritic mRNA transport by CPEB. *Genes Dev* **17**: 638–653. http://genesdev.cshlp.org/lookup/doi/10.1101/gad.1053003.

Huang Y, Ng FS, Jackson FR. 2015. Comparison of Larval and Adult Drosophila Astrocytes Reveals Stage-Specific Gene Expression Profiles. *G3 Genes|Genomes|Genetics* **5**: 551–558. https://academic.oup.com/g3journal/article/5/4/551/6025262.

Jeffery WR, Tomlinson CR, Brodeur RD. 1983. Localization of actin messenger RNA during early ascidian development. *Dev Biol* **99**: 408–17. http://www.ncbi.nlm.nih.gov/pubmed/6194032.

Kaloshi G, Mokhtari K, Carpentier C, Taillibert S, Lejeune J, Marie Y, Delattre J-Y, Godbout R, Sanson M. 2007. FABP7 expression in glioblastomas: relation to prognosis, invasion and EGFR status. *J Neurooncol* **84**: 245–248. http://link.springer.com/10.1007/s11060-007-9377-4.

Kano S, Choi EY, Dohi E, Agarwal S, Chang DJ, Wilson AM, Lo BD, Rose IVL, Gonzalez S, Imai T, et al. 2019. Glutathione S -transferases promote proinflammatory astrocyte-microglia communication during brain inflammation. *Sci Signal* **12**. https://www.science.org/doi/10.1126/scisignal.aar2124.

Kato K, Orihara-Ono M, Awasaki T. 2020. Multiple lineages enable robust development of the neuropil-glia architecture in adult Drosophila. *Development*. https://journals.biologists.com/dev/article/doi/10.1242/dev.184085/266858/Multiple-lineages-enable-robust-development-of-the.

Kim YS, Choi J, Yoon B-E. 2020. Neuron-Glia Interactions in Neurodevelopmental Disorders. *Cells* **9**: 2176. https://www.mdpi.com/2073-4409/9/10/2176.

Konstantinides N, Holguera I, Rossi AM, Escobar A, Dudragne L, Chen Y-C, Tran TN, Martínez Jaimes AM, Özel MN, Simon F, et al. 2022. A complete temporal transcription factor series in the fly visual system. *Nature* **604**: 316–322. https://www.nature.com/articles/s41586-022-04564-w.

Konstantinides N, Kapuralin K, Fadil C, Barboza L, Satija R, Desplan C. 2018. Phenotypic Convergence: Distinct Transcription Factors Regulate Common Terminal Features. *Cell* **174**: 622-635.e13. https://linkinghub.elsevier.com/retrieve/pii/S0092867418306330.

Kremer MC, Jung C, Batelli S, Rubin GM, Gaul U. 2017. The glia of the adult Drosophila nervous system. *Glia* **65**: 606–638. https://onlinelibrary.wiley.com/doi/10.1002/glia.23115.
Kügelgen N, Chekulaeva M. 2020. Conservation of a core neurite transcriptome across neuronal types and species. *WIREs RNA* **11**. https://onlinelibrary.wiley.com/doi/10.1002/wrna.1590.
Kurmangaliyev YZ, Yoo J, Valdes-Aleman J, Sanfilippo P, Zipursky SL. 2020. Transcriptional Programs of Circuit Assembly in the Drosophila Visual System. *Neuron* **108**: 1045-1057.e6. https://linkinghub.elsevier.com/retrieve/pii/S0896627320307741.
Li X, Erclik T, Bertet C, Chen Z, Voutev R, Venkatesh S, Morante J, Celik A, Desplan C. 2013. Temporal patterning of Drosophila medulla neuroblasts controls neural fates. *Nature* **498**: 456–462. http://www.nature.com/articles/nature12319.
Martin KC, Ephrussi A. 2009. mRNA Localization: Gene Expression in the Spatial Dimension. *Cell* **136**: 719–730. https://linkinghub.elsevier.com/retrieve/pii/S0092867409001263.
Matthews KA, Miller DFB, Kaufman TC. 1990. Functional implications of the unusual spatial distribution of a minor α-tubulin isotype in Drosophila: A common thread among chordotonal ligaments, developing muscle, and testis cyst cells. *Dev Biol* **137**: 171–183. https://linkinghub.elsevier.com/retrieve/pii/001216069090018E.
McMullen E, Weiler A, Becker HM, Schirmeier S. 2021. Plasticity of Carbohydrate Transport at the Blood-Brain Barrier. *Front Behav Neurosci* **14**. https://www.frontiersin.org/articles/10.3389/fnbeh.2020.612430/full.
Mirsaeidi M, Gidfar S, Vu A, Schraufnagel D. 2016. Annexins family: insights into their functions and potential role in pathogenesis of sarcoidosis. *J Transl Med* **14**: 89. http://translational-medicine.biomedcentral.com/articles/10.1186/s12967-016-0843-7.
Morante J, Vallejo DM, Desplan C, Dominguez M. 2013. Conserved miR-8/miR-200 Defines a Glial Niche that Controls Neuroepithelial Expansion and Neuroblast Transition. *Dev Cell* **27**: 174–187. https://linkinghub.elsevier.com/retrieve/pii/S1534580713005443.
Nakano R, Iwamura M, Obikawa A, Togane Y, Hara Y, Fukuhara T, Tomaru M, Takano-Shimizu T, Tsujimura H. 2019. Cortex glia clear dead young neurons via Drpr/dCed-6/Shark and Crk/Mbc/dCed-12 signaling pathways in the developing Drosophila optic lobe. *Dev Biol* **453**: 68–85. https://linkinghub.elsevier.com/retrieve/pii/S0012160618305645.
Omoto JJ, Yogi P, Hartenstein V. 2015. Origin and development of neuropil glia of the Drosophila larval and adult brain: Two distinct glial populations derived from separate progenitors. *Dev Biol* **404**: 2–20. https://linkinghub.elsevier.com/retrieve/pii/S0012160615001116.
Özel MN, Simon F, Jafari S, Holguera I, Chen YC, Benhra N, El-Danaf RN, Kapuralin K, Malin JA, Konstantinides N, et al. 2021. Neuronal diversity and convergence in a visual system developmental atlas. *Nature*.
Phipson B, Zappia L, Oshlack A. 2017. Gene length and detection bias in single cell

RNA sequencing protocols. *F1000Research* **6**: 595. https://f1000research.com/articles/6-595/v1.
Poeck B, Fischer S, Gunning D, Zipursky SL, Salecker I. 2001. Glial cells mediate target layer selection of retinal axons in the developing visual system of Drosophila. *Neuron*.
Qiu P. 2020. Embracing the dropouts in single-cell RNA-seq analysis. *Nat Commun* **11**: 1169. http://www.nature.com/articles/s41467-020-14976-9.
Richier B, Vijandi C de M, Mackensen S, Salecker I. 2017. Lapsyn controls branch extension and positioning of astrocyte-like glia in the Drosophila optic lobe. *Nat Commun* **8**: 317. http://www.nature.com/articles/s41467-017-00384-z.
Romero-Calderón R, Uhlenbrock G, Borycz J, Simon AF, Grygoruk A, Yee SK, Shyer A, Ackerson LC, Maidment NT, Meinertzhagen IA, et al. 2008. A Glial Variant of the Vesicular Monoamine Transporter Is Required To Store Histamine in the Drosophila Visual System ed. P.J. Dolph. *PLoS Genet* **4**: e1000245. https://dx.plos.org/10.1371/journal.pgen.1000245.
Saisawang C, Wongsantichon J, Ketterman AJ. 2012. A preliminary characterization of the cytosolic glutathione transferase proteome from Drosophila melanogaster. *Biochem J* **442**: 181–190. https://portlandpress.com/biochemj/article/442/1/181/80066/A-preliminary-characterization-of-the-cytosolic.
Schwarzkopf M, Liu MC, Schulte SJ, Ives R, Husain N, Choi HMT, Pierce NA. 2021. Hybridization chain reaction enables a unified approach to multiplexed, quantitative, high-resolution immunohistochemistry and in situ hybridization. *Development* **148**. https://journals.biologists.com/dev/article/148/22/dev199847/273470/Hybridization-chain-reaction-enables-a-unified.
Simon F, Konstantinides N. 2021. Single-cell transcriptomics in the Drosophila visual system: Advances and perspectives on cell identity regulation, connectivity, and neuronal diversity evolution. *Dev Biol* **479**: 107–122. https://linkinghub.elsevier.com/retrieve/pii/S0012160621001913.
Solito E, McArthur S, Christian H, Gavins F, Buckingham JC, Gillies GE. 2008. Annexin A1 in the brain – undiscovered roles? *Trends Pharmacol Sci* **29**: 135–142. https://linkinghub.elsevier.com/retrieve/pii/S0165614708000205.
Spéder P, Brand AH. 2018. Systemic and local cues drive neural stem cell niche remodelling during neurogenesis in Drosophila. *Elife* **7**. https://elifesciences.org/articles/30413.
Stogsdill JA, Kim K, Binan L, Farhi SL, Levin JZ, Arlotta P. 2022. Pyramidal neuron subtype diversity governs microglia states in the neocortex. *Nature* **608**: 750–756. https://www.nature.com/articles/s41586-022-05056-7.
Tix S, Eule E, Fischbach K-F, Benzer S. 1997. Glia in the chiasms and medulla of the Drosophila melanogaster optic lobes. *Cell Tissue Res* **289**: 397–409. http://link.springer.com/10.1007/s004410050886.
Viktorin G, Riebli N, Reichert H. 2013. A multipotent transit-amplifying neuroblast lineage in the central brain gives rise to optic lobe glial cells in Drosophila. *Dev Biol* **379**: 182–194. https://linkinghub.elsevier.com/retrieve/pii/S0012160613002005.

Wake H, Lee PR, Fields RD. 2011. Control of Local Protein Synthesis and Initial Events in Myelination by Action Potentials. *Science (80-)* **333**: 1647–1651. https://www.science.org/doi/10.1126/science.1206998.

Zenker J, Stettner M, Ruskamo S, Domènech-Estévez E, Baloui H, Médard J-J, Verheijen MHG, Brouwers JF, Kursula P, Kieseier BC, et al. 2014. A role of peripheral myelin protein 2 in lipid homeostasis of myelinating schwann cells. *Glia* **62**: 1502–1512. https://onlinelibrary.wiley.com/doi/10.1002/glia.22696.

Zhang HL, Eom T, Oleynikov Y, Shenoy SM, Liebelt DA, Dictenberg JB, Singer RH, Bassell GJ. 2001. Neurotrophin-Induced Transport of a β-Actin mRNP Complex Increases β-Actin Levels and Stimulates Growth Cone Motility. *Neuron* **31**: 261–275. https://linkinghub.elsevier.com/retrieve/pii/S0896627301003579.